

# Doubly-Iterative Sparsified MMSE Turbo Equalization for OTFS Modulation

Haotian Li, *Student Member, IEEE*, Qiyue Yu, *Senior Member, IEEE*

## Abstract

Currently, orthogonal time frequency space (OTFS) modulation has drawn much attention to reliable communications in high-mobility scenarios. This paper proposes a doubly-iterative sparsified minimum mean square error (DI-S-MMSE) turbo equalizer, which iteratively exchanges the extrinsic information between a soft-input-soft-input (SISO) MMSE estimator and a SISO decoder. Our proposed equalizer does not suffer from short loops and approaches the performance of the near-optimal symbol-wise maximum *a posteriori* (MAP) algorithm. To exploit the inherent sparsity of OTFS system, we resort to graph theory to investigate the sparsity pattern of the channel matrix, and propose two sparsification guidelines to reduce the complexity of calculating the matrix inverse at the MMSE estimator. Then, we apply two iterative algorithms to MMSE estimation, i.e., the Generalized Minimal Residual (GMRES) and Factorized Sparse Approximate Inverse (FSPAI) algorithms. The former is used at the initial turbo iteration, whose global convergence is proven in our equalizer, while the latter is used at the subsequent turbo iterations with the help of our proposed guidelines. Simulation results demonstrate that our equalizer has a linear order of complexity while the performance loss incurred by the sparsification is only 0.2 dB at  $10^{-4}$  bit error rate.

## Index Terms

Orthogonal time frequency space (OTFS), minimum mean square error (MMSE), turbo equalization, graph theory, iterative algorithms for sparse linear systems.

## I. INTRODUCTION

Next generation wireless communication systems are expected to accommodate various wireless applications in high-mobility scenarios, such as vehicle-to-vehicle (V2V), and high speed railway. In these scenarios, the performance of conventional orthogonal frequency division multiplexing (OFDM) is greatly degraded. To combat the Doppler spread, one of the appealing solutions is orthogonal time frequency space (OTFS) [1], [2], which has great potential for supporting reliable communications in high-mobility scenarios.

OTFS multiplexes the information symbols in the delay-Doppler (DD) domain instead of the time-frequency (TF) domain. Through a two-dimensional transform, OTFS spreads each symbol across the entire TF domain so that all symbols experience the same channel gain. Hence, OTFS has the potential of extracting full channel diversity, and greatly outperforms conventional OFDM systems [1], [3]–[6]. More importantly, the DD domain representation of wireless channel is inherently sparse and has lower variability than that in the TF domain, which facilitates channel estimation and significantly reduces the overhead [1], [7], [8].

However, these benefits of OTFS are obtained at the expense of prohibitive detection complexity. Therefore, many researchers have developed various low-complexity detectors by exploiting the sparsity of the wireless channel in the DD domain. In [9], the authors have proposed a linear minimum mean square error (LMMSE) receiver with a log-linear complexity order, which utilizes the sparsity and quasi-banded structure of the matrices. To further harvest the diversity gain, the authors of [3] have developed an iterative receiver based on message passing algorithm (MPA) with a linear complexity order, in which the interference is assumed to be Gaussian. Moreover, a hybrid maximum *a posteriori* (MAP) and parallel interference cancellation (PIC) detection (Hybrid-MAP-PIC) algorithm has been proposed in [10], whose performance approaches that of the near-optimal symbol-wise MAP algorithm with low complexity. However, due to the short loops in the factor graph that commonly exist in OTFS system, the MPA and Hybrid-MAP-PIC algorithm may fail to converge, resulting in undesirable performance degradation. To tackle this issue, a variational Bayes approach has been developed in [11], which can converge regardless of the short loops in the factor graph. Besides, the authors of [12] have investigated the design of OTFS detector based on approximate message passing (AMP), which handles short loops well with low complexity, and achieve a comparable bit error rate (BER) performance to the MMSE detection. In [13], a cross domain iterative detection of OTFS system has been proposed, which passes the extrinsic information between the time and DD domain. This detector can approach the performance of the maximum-likelihood (ML) sequence detection at the cost of a cubic complexity order.

The existing studies motivate us to achieve a desirable trade-off between the BER performance and complexity. In this paper, we propose a doubly-iterative sparsified MMSE (DI-S-MMSE) turbo equalizer, which consists of a sparsified soft-input-soft-output (SISO) MMSE estimator and a SISO decoder. It is observed that the overall computational complexity is dominated by computing the inverse of the covariance matrix of the received sequence for MMSE estimation.

To address this problem, our proposed equalizer sparsifies the covariance matrix so that its inverse can be derived with a linear complexity order. More importantly, our proposed equalizer does not suffer from the short loops as in the MPA [3] and SPA [10] detectors, and can approach the performance of the near-optimal symbol-wise MAP detector. The major contributions of this paper are summarized as follows.

- 1) We propose a doubly-iterative sparsified MMSE turbo equalizer, where we refer to the turbo iteration as the outer iteration. i.e., iteratively exchanging the extrinsic information between the MMSE estimator and the decoder. On the other hand, to reduce the detection complexity, we use two iterative algorithms to perform MMSE estimation, namely the Generalized Minimal Residual (GMRES) and Factorized Sparse Approximate Inverse (FSPAI) algorithms, which are referred to as inner iteration.
- 2) To fully exploit the inherent sparsity of the channel matrix in the DD domain, we resort to graph theory to analyze the sparsity pattern of the channel matrix. Based on graph theory, we propose two guidelines to sparsify the covariance matrix. In addition, considering the randomness of the channel matrix, we define the sparsity level of a random sparse matrix as the cumulative distribution function (CDF) of its node degrees. It is shown that the sparsity level of the inverse can be greatly improved by the proposed sparsification guidelines and therefore the detection complexity is significantly reduced.
- 3) At the initial outer iteration, computing the inverse is converted into solving the equivalent sparse linear systems via the GMRES algorithm. More importantly, we prove the global convergence of GMRES in our system. At the subsequent outer iterations, we resort to the proposed guidelines to sparsify the covariance matrix. Then, using the Hermitian positive definiteness of the covariance matrix, we modify FSPAI algorithm to approximately derive the Cholesky decomposition of the inverse. Simulation results demonstrate that the proposed equalizer greatly reduces the complexity with little performance degradation.

The remainder of this paper is organized as follows. In Section II, the system model of the proposed system is presented. Section III provides a brief overview of the proposed equalizer. Then, we analyze the sparsity pattern of the random sparse matrices and propose two sparsification guidelines based on graph theory in Section IV. Section V presents the iterative algorithms. The theoretical analysis is given in Section VI, and simulation results are presented in Section VII. Finally, some conclusions are drawn in Section VIII.

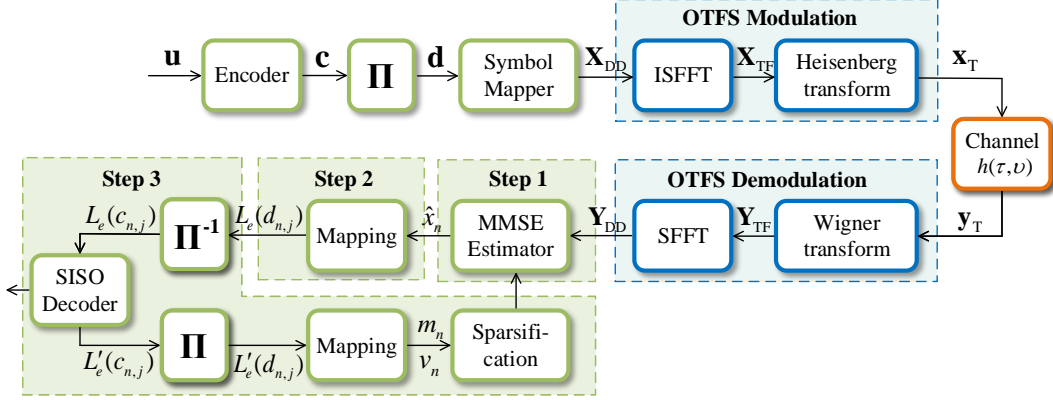


Fig. 1. A diagram of OTFS transceiver. where  $\Pi$  and  $\Pi^{-1}$  are the interleaver and deinterleaver respectively. Each iteration of the proposed equalizer consists of three steps: 1) perform MMSE estimation using the *a priori* information; 2) map the estimated symbols to the extrinsic information for the decoder; 3) after decoding, update means and variances, and sparsify the covariance matrix of the received sequence for the MMSE estimator.

*Notations:* Scalars, vectors and matrices are denoted by  $a$ ,  $\mathbf{a}$  and  $\mathbf{A}$  respectively.  $\mathbb{B}$ ,  $\mathbb{N}$ ,  $\mathbb{Z}$ ,  $\mathbb{R}$ ,  $\mathbb{R}^+$  and  $\mathbb{C}$  represent the set of all binary numbers, natural numbers, integers, real numbers, real positive numbers and complex numbers.  $\delta(\cdot)$  is the Dirac delta function.  $\lfloor a \rfloor$  denotes the largest integer less than or equal to  $a$ .  $\text{Re}\{a\}$  and  $\text{Im}\{a\}$  mean the real and imaginary parts of  $a$ , and  $a^*$  is the conjugate of  $a$ .  $\|\mathbf{a}\|$  represents the  $\ell_2$ -norm of a vector  $\mathbf{a}$ . The inner product of two vectors  $\mathbf{a}$  and  $\mathbf{b}$  is denoted by  $(\mathbf{a}, \mathbf{b})$ .  $\mathbf{A}(i, j)$  denotes the  $(i, j)$ -th element of  $\mathbf{A}$ . The transpose, conjugate, conjugate transpose and inverse of a matrix are represented by  $(\cdot)^T$ ,  $(\cdot)^*$ ,  $(\cdot)^H$  and  $(\cdot)^{-1}$ .  $\text{diag}[\mathbf{a}]$  denotes a diagonal matrix whose diagonal elements are  $\mathbf{a}$ , and  $\text{vec}(\cdot)$  represents the column-wise vectorization of a matrix.  $\mathcal{CN}(\mu, \sigma^2)$  denotes the circularly symmetric complex Gaussian distribution with mean  $\mu$  and variance  $\sigma^2$ . The expectation operator is denoted by  $\mathbb{E}\{\cdot\}$ . The covariance matrix of two vectors is represented by  $\text{Cov}\{\mathbf{x}, \mathbf{y}\} = \mathbb{E}\{\mathbf{x}\mathbf{y}^H\} - \mathbb{E}\{\mathbf{x}\}\mathbb{E}\{\mathbf{y}^H\}$ .  $\mathcal{O}(\cdot)$  denotes the order of asymptotic time complexity.  $|\mathcal{A}|$  denotes the cardinality of a set  $\mathcal{A}$ .

## II. SYSTEM MODEL

### A. OTFS Transmitter

The diagram of OTFS system is shown in Fig. 1. The bitstream  $\mathbf{u} \in \mathbb{B}^{K_1}$  is encoded by an encoder with a generator matrix  $\mathbf{G}$  whose code rate is  $R_c$ , through which an encoded vector  $\mathbf{c} = \mathbf{G}\mathbf{u} \in \mathbb{B}^{K_2}$  is obtained, where  $K_1 = K_2 \cdot R_c$ . Then,  $\mathbf{c}$  is interleaved to  $\mathbf{d} \in \mathbb{B}^{K_2}$ , and mapped to the symbol sequence  $\mathbf{x} \in \mathbb{C}^{K_3}$  from the symbol alphabet  $\mathcal{S}$ , where  $K_3 = K_2 / \log_2(|\mathcal{S}|)$ . Then  $\mathbf{x}$  is arranged into an  $M \times N$  DD domain matrix  $\mathbf{X}_{\text{DD}}$  column by column with  $K_3 = MN$ , where the delay and Doppler dimensions contain  $M$  and  $N$  samples respectively.

Next, the inverse symplectic finite Fourier transform (ISFFT) performs an  $M$ -point FFT along the delay dimension and an  $N$ -point IFFT along the Doppler dimension to yield the TF domain transmit symbols matrix  $\mathbf{X}_{\text{TF}} \in \mathbb{C}^{M \times N}$  as [14]

$$\mathbf{X}_{\text{TF}} = \mathbf{F}_M \mathbf{X}_{\text{DD}} \mathbf{F}_N^H, \quad (1)$$

where  $\mathbf{F}_M$  denotes the  $M$ -point DFT matrix and  $\mathbf{F}_N^H$  denotes the  $N$ -point IDFT matrix. Here,  $NT$  and  $M\Delta f$  represent the time duration and bandwidth respectively, where the subcarrier spacing is  $\Delta f$  (Hz) and the time interval is  $T$  (seconds).

After the ISFFT, the Heisenberg transform performs an  $M$ -point IFFT along each column of  $\mathbf{X}_{\text{TF}}$  and applies the pulse shaping waveform  $g_{\text{tx}}(t)$  of duration  $[0, T)$ . Then, the obtained time domain transmit matrix  $\mathbf{X}_{\text{T}}$  can be denoted by [14]

$$\mathbf{X}_{\text{T}} = \mathbf{G}_{\text{tx}} \mathbf{F}_M^H \mathbf{X}_{\text{TF}} = \mathbf{G}_{\text{tx}} \mathbf{X}_{\text{DD}} \mathbf{F}_N^H, \quad (2)$$

where the diagonal elements of  $\mathbf{G}_{\text{tx}}$  are samples of  $g_{\text{tx}}(t)$  with sampling interval  $T/M$ , i.e.,  $\mathbf{G}_{\text{tx}} = \text{diag} [g_{\text{tx}}(0), g_{\text{tx}}(T/M), \dots, g_{\text{tx}}((M-1)T/M)] \in \mathbb{C}^{M \times M}$ . This paper only considers the rectangular waveform, and thereby  $\mathbf{G}_{\text{tx}}$  is simplified as the identity matrix  $\mathbf{I}_M$ . Then, the transmit signal can be vectorized as  $\mathbf{x}_{\text{T}} = (\mathbf{F}_N^H \otimes \mathbf{G}_{\text{tx}}) \mathbf{x} = (\mathbf{F}_N^H \otimes \mathbf{I}_M) \mathbf{x}$ , where  $\mathbf{x}_{\text{T}} = \text{vec}(\mathbf{X}_{\text{T}}) \in \mathbb{C}^{MN}$  and  $\otimes$  represents the kronecker product. Such a vector of length  $MN$  is termed an OTFS frame [1]. A cyclic prefix (CP) of length  $L$  is appended to each OTFS frame, and after digital to analog conversion, the time domain signal  $x_{\text{T}}(t)$  is transmitted into the time-varying channel.

### B. Channel Model

The channel impulse response can be characterized as  $h(\tau, \nu)$  with delay  $\tau$  and Doppler  $\nu$

$$h(\tau, \nu) = \sum_{p=1}^P h_p \delta(\tau - \tau_p) \delta(\nu - \nu_p), \quad (3)$$

where  $h_p, \tau_p$  and  $\nu_p$  represent the channel gain, delay and Doppler shift of the  $p$ -th path for  $p = 1, \dots, P$ , and  $P$  is the number of paths [3]. Here,  $\tau_p = l_p/(M\Delta f)$  and  $\nu_p = k_p/(NT)$ , where the delay indices  $l_p$  and Doppler shift indices  $k_p$  are assumed to be integers. This assumption holds when  $M$  and  $N$  are large. The aforementioned length of the CP should be larger than the maximum delay, i.e.,  $L > \tau_{\text{max}} M\Delta f$ . According to [1], the received signal  $y_{\text{T}}(t)$  is

$$y_{\text{T}}(t) = \iint h(\tau, \nu) e^{j2\pi\nu(t-\tau)} x_{\text{T}}(t-\tau) d\tau d\nu + z_{\text{T}}(t), \quad (4)$$

where  $z_{\text{T}}(t)$  is the additive white Gaussian noise (AWGN) in the time domain, which is distributed as  $\mathcal{CN}(0, N_0)$ . After CP is removed, the received signal is sampled with interval  $T/M$ . By substituting (3), the discrete received signal is obtained as [14]

$$y_T(n) = \sum_{p=1}^P h_p e^{j2\pi \frac{k_p(n-l_p)}{MN}} x_T([n-l_p]_{MN}) + z_T(n), \quad (5)$$

where  $n = 1, \dots, MN$  and  $[\cdot]_{MN}$  represents the modulo- $MN$  operation. From (5), the time domain effective channel matrix  $\mathbf{H}_T \in \mathbb{C}^{MN \times MN}$  can be written as [14]

$$\mathbf{H}_T = \sum_{p=1}^P h_p \mathbf{\Pi}^{l_p} \mathbf{\Delta}^{k_p}, \quad (6)$$

where  $\mathbf{\Pi}$  is a permutation matrix (forward cyclic shift) and represents the effect of delay

$$\mathbf{\Pi}_{MN} = \begin{bmatrix} 0 & \cdots & 0 & 1 \\ 1 & \cdots & 0 & 0 \\ \vdots & \ddots & \ddots & \vdots \\ 0 & \cdots & 1 & 0 \end{bmatrix}_{MN \times MN}, \quad (7)$$

and  $\mathbf{\Delta}$  models the Doppler effect and introduces an extra frequency shift, which is an  $MN \times MN$  diagonal matrix as  $\mathbf{\Delta} = \text{diag}[\omega^0, \omega^1, \dots, \omega^{MN-1}]$  with  $\omega = e^{j\frac{2\pi}{MN}}$ . In (6), each path incurs an  $l_p$ -step cyclic time shift, represented by  $\mathbf{\Pi}^{l_p}$ , along with a frequency shift  $k_p$  of the transmit signal  $\mathbf{x}_T$ , represented by  $\mathbf{\Delta}^{k_p}$ . In this way, the received signal  $\mathbf{y}_T \in \mathbb{C}^{MN}$  of (5) is given by

$$\mathbf{y}_T = \mathbf{H}_T \mathbf{x}_T + \mathbf{z}_T, \quad (8)$$

where  $\mathbf{z}_T \in \mathbb{C}^{MN}$  is the AWGN vector.

### C. OTFS Receiver

At the receiver,  $\mathbf{y}_T$  is rearranged into an  $M \times N$  matrix  $\mathbf{Y}_T$  column by column. Similarly, we consider rectangular received pulse shaping waveform. Then, an  $M$ -point FFT operation is applied to each column of  $\mathbf{Y}_T$  to obtain the TF domain received signal  $\mathbf{Y}_{TF} \in \mathbb{C}^{M \times N}$  as

$$\mathbf{Y}_{TF} = \mathbf{F}_M \mathbf{G}_{rx} \mathbf{Y}_T = \mathbf{F}_M \mathbf{I}_M \mathbf{Y}_T. \quad (9)$$

Afterwards, the SFFT is performed, which consists of an  $M$ -point IFFT of columns and an  $N$ -point FFT of rows. Thus, by substituting (9), the DD domain received matrix  $\mathbf{Y}_{DD}$  is yielded as  $\mathbf{Y}_{DD} = \mathbf{F}_M^H \mathbf{Y}_{TF} \mathbf{F}_N = \mathbf{I}_M \mathbf{Y}_T \mathbf{F}_N$ , whose vectorized form is  $\mathbf{y} = \text{vec}(\mathbf{Y}_{DD}) = (\mathbf{F}_N \otimes \mathbf{I}_M) \mathbf{y}_T$ . Then, the transmit DD domain vector  $\mathbf{x}$  and the received DD domain vector  $\mathbf{y}$  are related as

$$\mathbf{y} = (\mathbf{F}_N \otimes \mathbf{I}_M) \mathbf{H}_T (\mathbf{F}_N^H \otimes \mathbf{I}_M) \mathbf{x} + (\mathbf{F}_N \otimes \mathbf{I}_M) \mathbf{z}_T = \mathbf{H}_{DD} \mathbf{x} + \mathbf{z}, \quad (10)$$

where  $\mathbf{z}$  is the DD domain noise vector, and the effective DD domain channel matrix is

$$\mathbf{H}_{DD} = (\mathbf{F}_N \otimes \mathbf{I}_M) \mathbf{H}_T (\mathbf{F}_N^H \otimes \mathbf{I}_M) = \sum_{p=1}^P \mathbf{H}_{DD}^{(p)}, \quad (11)$$

where the  $p$ -th component  $\mathbf{H}_{DD}^{(p)} \in \mathbb{C}^{MN \times MN}$  is caused by the  $p$ -th path. It has been proven that

$$\mathbf{H}_{\text{DD}}^{(p)}(a, b) = \begin{cases} \omega^{k_p[l_a - l_p]_M - k_a M}, & \text{if } b = [l_a - l_p]_M + M[k_a - k_p]_N \text{ and } l_a < l_p \\ \omega^{k_p[l_a - l_p]_M}, & \text{if } b = [l_a - l_p]_M + M[k_a - k_p]_N \text{ and } l_a \geq l_p \\ 0, & \text{otherwise.} \end{cases} \quad (12)$$

where  $0 \leq a, b \leq MN - 1$ ,  $k_a = \lfloor a/M \rfloor$  and  $l_a = a - k_a M$  [14]. Apparently,  $\mathbf{H}_{\text{DD}}^{(p)}$  contains only one nonzero element in each row and column, and thus  $\mathbf{H}_{\text{DD}}$  is a sparse matrix with  $P$  nonzero elements in each row and column. In what follows, the received sequence  $\mathbf{y}$  is fed into the turbo equalizer to recover the information bits. In practice, the size of an OTFS frame, i.e.,  $MN$  is usually very large. Therefore, a low-complexity equalizer is necessary.

### III. DOUBLY-ITERATIVE SPARSIFIED MMSE TURBO EQUALIZER

This paper proposes a doubly-iterative sparsified MMSE (DI-S-MMSE) turbo equalizer, which is composed of a SISO MMSE estimator and a SISO decoder. The proposed equalizer has a doubly iterative structure, i.e., the outer and inner iteration. The outer iteration is operated by passing soft information between the MMSE estimator and the decoder iteratively; the inner iteration is performed inside the MMSE estimator to reduce the computational cost by means of two iterative algorithms, i.e., the GMRES algorithm at the initial outer iteration and the FSPA algorithm at the subsequent outer iterations. This section mainly focuses on the outer iteration, and the following sections will investigate the sparsification methods and the iterative algorithms.

#### A. An overview of the outer iteration

As shown in Fig. 1, the outer iteration of our proposed equalizer consists of three steps: 1) perform MMSE estimation using the *a priori* information; 2) calculate the extrinsic information for the decoder; 3) after decoding, update means and variances, and sparsify the covariance matrix for the MMSE estimator. In this paper, we use quadrature phase shift keying (QPSK) with alphabet  $\mathcal{S} = \{s_1 = (1+i)/\sqrt{2}, s_2 = (1-i)/\sqrt{2}, s_3 = (-1+i)/\sqrt{2}, s_4 = (-1-i)/\sqrt{2}\}$ . Here,  $s_k$  for  $k = 1, \dots, 4$  represents the  $k$ -th constellation, whose corresponding two bits  $\mathbf{s}_k = [s_{k,1}, s_{k,2}]$  are  $[0, 0]$ ,  $[0, 1]$ ,  $[1, 0]$  and  $[1, 1]$  respectively.

The first step is to estimate the transmit symbols from the received sequence  $\mathbf{y}$  by using the MMSE estimator. The input of the MMSE estimator consists of the mean  $m_n = \mathbb{E}\{x_n\}$  and the variance  $v_n = \mathbb{E}\{|x_n - m_n|^2\}$  of each symbol  $x_n$  for  $n = 1, \dots, MN$ . To minimize the mean square error (MSE)  $\mathbb{E}\{\|\mathbf{x} - \hat{\mathbf{x}}\|^2\}$ , the estimator derives the estimated symbol  $\hat{x}_n$  from  $\mathbf{y}$  as [15]

$$\hat{x}_n = m_n + \text{Cov}\{x_n, \mathbf{y}\} \text{Cov}\{\mathbf{y}, \mathbf{y}\}^{-1} (\mathbf{y} - \mathbb{E}\{\mathbf{y}\}). \quad (13)$$

For notational convenience, the covariance matrix of the received sequence  $\mathbf{y}$  is denoted by  $\mathbf{A} = \text{Cov}\{\mathbf{y}, \mathbf{y}\}$ , and computing its inverse largely dominates the complexity of our equalizer.

Next, the estimated symbol  $\hat{x}_n$  is mapped to its corresponding log-likelihood ratio (LLR) for the decoder. To harvest the potential full channel diversity gain, the *a posteriori* probability of each bit with respect to the entire received sequence  $\mathbf{y}$  is desirable, i.e.,  $P(d_{n,j}|\mathbf{y})$ , where  $\mathbf{d}_n = [d_{n,1}, d_{n,2}]$  denotes the interleaved bits corresponding to the symbol  $x_n \in \mathcal{S}$  and  $j = 1, 2$ . However, computing  $P(d_{n,j}|\mathbf{y})$  is extremely time-consuming, especially when  $M$  and  $N$  are large. Therefore, [16] inventively introduces the *a posteriori* probability with respect to the estimated symbol  $P(d_{n,j}|\hat{x}_n)$  to approximate  $P(d_{n,j}|\mathbf{y})$ . The LLR of  $P(d_{n,j}|\hat{x}_n)$  is defined as

$$\begin{aligned} L(d_{n,j}|\hat{x}_n) &\triangleq \ln \frac{P(d_{n,j} = 0|\hat{x}_n)}{P(d_{n,j} = 1|\hat{x}_n)} = \ln \frac{\sum_{\forall \mathbf{d}_n: d_{n,j}=0} p(\hat{x}_n|\mathbf{d}_n)P(\mathbf{d}_n)}{\sum_{\forall \mathbf{d}_n: d_{n,j}=1} p(\hat{x}_n|\mathbf{d}_n)P(\mathbf{d}_n)} \\ &= \ln \frac{\sum_{\forall \mathbf{d}_n: d_{n,j}=0} p(\hat{x}_n|\mathbf{d}_n) \prod_{\forall j': j' \neq j} P(d_{n,j'})}{\sum_{\forall \mathbf{d}_n: d_{n,j}=1} p(\hat{x}_n|\mathbf{d}_n) \prod_{\forall j': j' \neq j} P(d_{n,j'})} + \ln \frac{P(d_{n,j} = 0)}{P(d_{n,j} = 1)}, \end{aligned} \quad (14)$$

where  $j' = 1, 2$ . The first term of (14) is defined as the extrinsic LLR  $L_e(d_{n,j})$ , and the second term is defined as the *a priori* LLR  $L(d_{n,j})$ , which is derived from the decoder. It is worth noting that  $L_e(d_{n,j})$  and  $L(d_{n,j})$  should be strictly independent.

Last, the estimator outputs the extrinsic information, which serves as the *a priori* information of the decoder. Thereafter, the decoder further mitigates the interference, and feeds the extrinsic information back to the estimator, from which new means and variances are obtained. Before we start another outer iteration, the covariance matrix  $\mathbf{A}$  is sparsified to reduce the detection complexity. In the following, we will give a detailed description of these three steps.

### B. Step 1: MMSE Estimation Using the A Priori Information

At the initial iteration, it is assumed that  $m_n = 0$  and  $v_n = 1$ , while at the subsequent iterations, means and variances are provided by the decoder. By substituting (10), we have

$$\text{Cov}\{\mathbf{x}, \mathbf{x}\} = \text{diag}[v_1, \dots, v_{MN}] \triangleq \mathbf{V}, \quad (15a)$$

$$\text{Cov}\{\mathbf{z}, \mathbf{z}\} = (\mathbf{F}_N \otimes \mathbf{I}_M) \text{Cov}\{\mathbf{z}_T, \mathbf{z}_T\} (\mathbf{F}_N^H \otimes \mathbf{I}_M) = N_0 \mathbf{I}, \quad (15b)$$

$$\text{Cov}\{\mathbf{y}, \mathbf{y}\} = \mathbf{A} = \mathbf{H}_{DD} \mathbf{V} \mathbf{H}_{DD}^H + N_0 \mathbf{I}, \quad (15c)$$

where (15a) is obtained due to the assumption that the transmitted symbols are independent, which approximately holds due to the interleaver; (15b) is derived from  $\text{Cov}\{\mathbf{z}_T, \mathbf{z}_T\} = N_0 \mathbf{I}$  and  $(\mathbf{F}_N \otimes \mathbf{I}_M) (\mathbf{F}_N^H \otimes \mathbf{I}_M) = \mathbf{I}$  where the subscript of  $\mathbf{I}_{MN}$  can be omitted without ambiguity. Moreover, we derive  $\text{Cov}\{x_n, \mathbf{y}\} = \text{Cov}\{x_n, \mathbf{x}\} \mathbf{H}_{DD}^H = v_n \mathbf{h}_n^H$ , where  $\mathbf{h}_n$  represents the  $n$ -th



column of  $\mathbf{H}_{\text{DD}}$ . By substituting  $\text{Cov}\{\mathbf{y}, \mathbf{y}\}$  and  $\text{Cov}\{x_n, \mathbf{y}\}$  into (13), the estimated symbol  $\hat{x}_n$  is derived as

$$\hat{x}_n = m_n + v_n \mathbf{h}_n^H \mathbf{A}^{-1} (\mathbf{y} - \mathbf{H}_{\text{DD}} \mathbf{m}), \quad (16)$$

where  $\mathbf{m} = [m_1, \dots, m_{MN}]$  denotes the vector of means.

Note that the derivation of  $\hat{x}_n$  relies on the *a priori* knowledge  $L(d_{n,j})$ , so that the resultant  $L_e(d_{n,j})$  derived from  $\hat{x}_n$  is not independent of  $L(d_{n,j})$ . Thus, (16) is modified as [16]

$$\hat{x}_n = 0 + 1 \cdot \mathbf{h}_n^H (\mathbf{A} + (1 - v_n) \mathbf{h}_n \mathbf{h}_n^H)^{-1} (\mathbf{y} - \mathbf{H}_{\text{DD}} \mathbf{m} + m_n \mathbf{h}_n), \quad (17)$$

where  $\hat{x}_n$  excludes its own *a priori* knowledge by setting  $m_n = 0$  and  $v_n = 1$ . To avoid computing the inverse in (17) repeatedly for each  $\hat{x}_n$ , the Woodbury matrix identity [17] is utilized as

$$\begin{aligned} \mathbf{h}_n^H (\mathbf{A} + (1 - v_n) \mathbf{h}_n \mathbf{h}_n^H)^{-1} &= \mathbf{h}_n^H \mathbf{A}^{-1} - \mathbf{h}_n^H \mathbf{A}^{-1} \mathbf{h}_n [(1 - v_n)^{-1} + \mathbf{h}_n^H \mathbf{A}^{-1} \mathbf{h}_n]^{-1} \mathbf{h}_n^H \mathbf{A}^{-1} \\ &= [1 + (1 - v_n) \xi_n]^{-1} \mathbf{h}_n^H \mathbf{A}^{-1}, \end{aligned} \quad (18)$$

where  $\xi_n = \mathbf{h}_n^H \mathbf{A}^{-1} \mathbf{h}_n$ . Then, by substituting (18) into (17), the estimated symbol is

$$\hat{x}_n = \frac{\mathbf{h}_n^H \mathbf{A}^{-1} (\mathbf{y} - \mathbf{H}_{\text{DD}} \mathbf{m}) + m_n \xi_n}{1 + (1 - v_n) \xi_n}. \quad (19)$$

From (19), we observe that  $\mathbf{A}^{-1}$  is used twice, i.e.,  $\mathbf{h}_n^H \mathbf{A}^{-1} (\mathbf{y} - \mathbf{H}_{\text{DD}} \mathbf{m})$  and  $\xi_n$ , which dominates the complexity of MMSE estimation.

### C. Step 2: Calculate the Extrinsic Information for the Decoder

To calculate  $L_e(d_{n,j})$  in (14),  $p(\hat{x}_n | \mathbf{d}_n = \mathbf{s}_k)$  can be assumed to be Gaussian distribution as  $p(\hat{x}_n | \mathbf{d}_n = \mathbf{s}_k) = p(\hat{x}_n | x_n = s_k) = 1/(\pi \sigma_{n,k}^2) \exp(-|\hat{x}_n - \mu_{n,k}|^2 / \sigma_{n,k}^2)$ . Here,  $\mu_{n,k} \triangleq \mathbb{E}\{\hat{x}_n | x_n = s_k\}$  and  $\sigma_{n,k}^2 \triangleq \mathbb{E}\{|\hat{x}_n - \mu_{n,k}|^2 | x_n = s_k\}$  are the mean and variance of the estimation error  $e_{n,k} = \hat{x}_n - s_k$ . According to (19),  $\mu_{n,k}$  and  $\sigma_{n,k}^2$  are given by

$$\begin{aligned} \mu_{n,k} &= \frac{1}{1 + (1 - v_n) \xi_n} [\mathbf{h}_n^H \mathbf{A}^{-1} (\mathbb{E}\{\mathbf{y} | x_n = s_k\} - \mathbf{H}_{\text{DD}} \mathbf{m}) + m_n \xi_n] \\ &= \frac{1}{1 + (1 - v_n) \xi_n} \mathbf{h}_n^H \mathbf{A}^{-1} \mathbf{h}_n s_k = \frac{\xi_n s_k}{1 + (1 - v_n) \xi_n}, \end{aligned} \quad (20)$$

$$\begin{aligned} \sigma_{n,k}^2 &= \frac{1}{[1 + (1 - v_n) \xi_n]^2} \mathbf{h}_n^H \mathbf{A}^{-1} \text{Cov}\{\mathbf{y}, \mathbf{y} | x_n = s_k\} (\mathbf{A}^{-1})^H \mathbf{h}_n \\ &= \frac{1}{[1 + (1 - v_n) \xi_n]^2} (\xi_n^* - v_n \xi_n \xi_n^*) \stackrel{(a)}{=} \frac{\xi_n (1 - v_n \xi_n)}{[1 + (1 - v_n) \xi_n]^2}, \end{aligned} \quad (21)$$

where (a) follows from the fact that  $\mathbf{A}$  is Hermitian, and thus  $\xi_n$  is a real number. By substituting (20) and (21) into the extrinsic LLR of (14),  $L_e(d_{n,j})$  for  $j = 1, 2$  are derived as [16]

$$L_e(d_{n,1}) = \frac{\sqrt{8}[1 + (1 - v_n)\xi_n]\text{Re}\{\hat{x}_n\}}{1 - v_n\xi_n}, \quad L_e(d_{n,2}) = \frac{\sqrt{8}[1 + (1 - v_n)\xi_n]\text{Im}\{\hat{x}_n\}}{1 - v_n\xi_n}. \quad (22)$$

Then,  $L_e(c_{n,j})$  is deinterleaved into  $L_e(d_{n,j})$ , and serves as the *a priori* information of the decoder.

#### D. Step 3: Update Means and Variances and Sparsify the Covariance Matrix

After decoding, the decoder outputs new extrinsic information  $L'_e(c_{n,j})$ . Through interleaver,  $L'_e(d_{n,j})$  is obtained and fed back to the estimator. Considering the definition of LLR,  $P(x_n = s_k)$  can be readily derived as

$$P(x_n = s_k) = \prod_{j=1}^2 P(d_{n,j} = s_{k,j}) = \prod_{j=1}^2 \frac{1}{2} \cdot \left[ 1 - \text{sgn}(s_{k,j} - \frac{1}{2}) \cdot \tanh\left(\frac{L'_e(d_{n,j})}{2}\right) \right], \quad (23)$$

where  $\text{sgn}(\cdot)$  is the sign function. From  $\mathcal{S}$ , new means and variances are obtained as

$$m_n = \sum_{k=1}^4 s_k \cdot P(x_n = s_k) = \frac{1}{\sqrt{2}} \left[ \tanh\left(\frac{L'_e(d_{n,1})}{2}\right) + i \cdot \tanh\left(\frac{L'_e(d_{n,2})}{2}\right) \right], \quad (24a)$$

$$v_n = \sum_{k=1}^4 |x_n - m_n|^2 P(x_n = s_k) = 1 - |m_n|^2. \quad (24b)$$

At the end of an outer iteration, we sparsify  $\mathbf{A}$  according to some guidelines as introduced in the next section.

### IV. SPARSIFICATION OF THE COVARIANCE MATRIX BASED ON GRAPH THEORY

As mentioned before, high complexity of the proposed equalizer is mainly caused by computing  $\mathbf{A}^{-1}$  in MMSE estimation, since  $\mathbf{A}$  is an  $MN \times MN$  random matrix, and  $MN$  is typically large. For example, if we have  $M = 64$  and  $N = 32$ , directly calculating  $\mathbf{A}^{-1}$  takes roughly  $(MN)^3 = 2^{33}$  complex multiplications. According to (15c),  $\mathbf{A}$  is a function of the random sparse matrix  $\mathbf{H}_{\text{DD}}$  so that  $\mathbf{A}$  is also a random sparse matrix. Unfortunately, the sparsity of  $\mathbf{A}$  cannot guarantee that  $\mathbf{A}^{-1}$  is also sparse. On the contrary, the inverse  $\mathbf{A}^{-1}$  is dense in most cases. Hence, in this section, we resort to graph theory to provide some insight into the sparsity pattern of  $\mathbf{A}$ , and propose some guidelines to sparsify  $\mathbf{A}$  so that  $\mathbf{A}^{-1}$  can be approximated as a sparse matrix and thus the detection complexity can be greatly reduced.

#### A. Sparsification Guidelines Based on Graph Theory

We first define the sparsity pattern of random sparse matrices for ease of further analysis.

**Definition 1.** (*Sparsity pattern*) Let  $\mathbf{S} \in \mathbb{C}^{N_s \times N_s}$  be a random sparse matrix. The sparsity pattern of  $\mathbf{S}$  is denoted by  $\text{sp}(\mathbf{S}) \in \mathbb{B}^{N_s \times N_s}$  to extract locations of nonzero elements, where the  $(i, j)$ -th element of  $\text{sp}(\mathbf{S})$  is set to be one if and only if  $\mathbf{S}(i, j) \neq 0$ .

In our system, we only focus on  $\mathbf{A}$  which is a Hermitian matrix, and has a symmetric sparsity pattern. Hence, we consider the case where  $\text{sp}(\mathbf{S})$  is symmetric in the following. The sparsity pattern of  $\mathbf{S}$  can be easily illustrated by its graph, denoted by  $\mathcal{G}(\mathcal{N}, \mathcal{E})$ , which consists of a set of nodes  $\mathcal{N}$  and a set of edges  $\mathcal{E}$  between nodes [18]. Here,  $\mathcal{N}$  contains  $N_S$  nodes that represent the corresponding row or column indices of  $\mathbf{S}$ ; the edge set  $\mathcal{E}$  includes all the undirected lines connecting from node  $i$  to node  $j$  if  $\mathbf{S}(i, j)$  and  $\mathbf{S}(j, i)$  are both nonzero due to the symmetry of  $\text{sp}(\mathbf{A})$ . The number of edges connected to a node is defined as the degree, denoted by  $D$ .

On the other hand, we need to take the randomness of  $\mathbf{S}$  into account. Since  $\mathbf{S}$  is a random sparse matrix, degree of its nodes is a discrete random variable, denoted by  $\tilde{\varphi}$ , where  $0 \leq \tilde{\varphi} \leq N_S - 1$ . Then, the sparsity level of  $\mathbf{S}$  is statistically measured as follows.

**Definition 2.** (*Sparsity level*) For a random sparse matrix  $\mathbf{S}$ , let  $F_{\tilde{\varphi}}(D) = P(\tilde{\varphi} \leq D)$  denote the CDF of  $\tilde{\varphi}$ , where  $D$  denotes a specific value of degrees and  $D = 0, 1, \dots, N_S - 1$ . We define  $F_{\tilde{\varphi}}(D)$  as the sparsity level of  $\mathbf{S}$ .

The sparsity level of  $\mathbf{S}^{-1}$  dictates the average complexity of our equalizer rather than that of  $\mathbf{S}$ . Hence, we only focus on the sparsity level of  $\mathbf{S}^{-1}$  in the following. Similarly, the node degree of  $\mathbf{S}^{-1}$  is also a random variable, denoted by  $\varphi$ . The node degrees  $\varphi$  are expected to concentrate around a small value for ease of deriving  $\mathbf{S}^{-1}$ . Specially, if node degrees of  $\mathbf{S}^{-1}$  are all equal to zero, i.e.,  $F_{\varphi}(0) = 1$ ,  $\mathbf{S}^{-1}$  is reduced to a diagonal matrix and thus can be derived with a complexity order  $\mathcal{O}(N_S)$ . Moreover, for two random sparse nonsingular matrices  $\mathbf{S}_1$  and  $\mathbf{S}_2$ , let  $\varphi_1$  and  $\varphi_2$  denote the node degrees of  $\mathbf{S}_1^{-1}$  and  $\mathbf{S}_2^{-1}$  respectively. If their sparsity levels satisfy  $F_{\varphi_1}(D) > F_{\varphi_2}(D)$  for any  $D$ , then  $\mathbf{S}_1^{-1}$  is sparser than  $\mathbf{S}_2^{-1}$ .

Next, based on graph theory, we propose two guidelines to sparsify  $\mathbf{S}$  from the edge and node aspects respectively so that the complexity of deriving  $\mathbf{S}^{-1}$  can be greatly reduced.

- 1) **Guideline 1** (Sparsify  $\mathbf{S}$  from edge constraint): Normalize the diagonal elements of  $\mathbf{S}$  through Jacobi scaling as  $\tilde{\mathbf{S}} = \mathbf{J}^{-\frac{1}{2}} \mathbf{S} \mathbf{J}^{-\frac{1}{2}}$ , where  $\mathbf{J}$  is a diagonal matrix and  $\mathbf{J}(i, i) = |\mathbf{S}(i, i)|$  for  $i = 1, \dots, N_S$  [19]. Then, if an edge satisfies  $|\tilde{\mathbf{S}}(i, j)| \leq \epsilon_S$ , it indicates that this edge is trivial and can be eliminated. Here,  $\epsilon_S$  is an appropriate threshold, and it is preferable to let  $\epsilon_S \ll 1$  in case of significant performance degradation;
- 2) **Guideline 2** (Sparsify  $\mathbf{S}$  from node constraint): If the degree of a node is smaller than a threshold  $\epsilon_D$ , i.e.,  $D \leq \epsilon_D$ , this node can be disconnected from other nodes. To avoid incurring too much imprecision,  $\epsilon_D$  should be much smaller than the maximum degree.

The first guideline deals with edges whose magnitude is negligible relative to the corresponding diagonal element, which have little impact on the computation of  $\mathbf{S}^{-1}$ . Moreover, we use the Jacobi scaling to normalize the diagonal elements for ease of choosing  $\epsilon_A$ . By guideline 1, when the diagonal elements of  $\mathbf{S}$  have larger magnitude than most of the off-diagonal elements,  $\mathbf{S}$  can be greatly sparsified. The second guideline further enhances the sparsity level of  $\mathbf{S}^{-1}$  via isolating the nodes with small degrees, since these nodes are hardly related with other nodes.

According to the guidelines, a smaller  $\epsilon_S$  and a larger  $\epsilon_D$  result in a sparser  $\mathbf{S}^{-1}$  at the cost of performance loss. Hence,  $\epsilon_S$  and  $\epsilon_D$  should be carefully chosen to strike a balance between the complexity of calculating  $\mathbf{S}^{-1}$  and performance loss.

### B. Apply the Sparsification Guidelines to the Proposed Equalizer

Now, we apply the proposed guidelines to our equalizer to reduce the complexity. According to (11) and (12),  $\mathbf{H}_{\text{DD}}$  is the sum of  $\mathbf{H}_{\text{DD}}^{(p)}$ , which contains only one nonzero element in each row and column whose sparsity pattern is given by

$$\text{sp}(\mathbf{H}_{\text{DD}}^{(p)}) = \mathbf{\Pi}_N^{k_p} \otimes \mathbf{\Pi}_M^{l_p}. \quad (25)$$

Then, the sparsity pattern of  $\mathbf{A}$  can be obtained as

$$\begin{aligned} \text{sp}(\mathbf{A}) &= \text{sp}(\mathbf{H}_{\text{DD}} \mathbf{V} \mathbf{H}_{\text{DD}}^{\text{H}} + N_0 \mathbf{I}) = \text{sp} \left( \sum_{p=1}^P \mathbf{\Pi}_N^{k_p} \otimes \mathbf{\Pi}_M^{l_p} \cdot \sum_{p'=1}^P \mathbf{\Pi}_N^{-k_{p'}} \otimes \mathbf{\Pi}_M^{-l_{p'}} \right), \\ &= \text{sp} \left( \sum_{p=1}^P \sum_{p'=1}^P \mathbf{\Pi}_N^{k_p - k_{p'}} \otimes \mathbf{\Pi}_M^{l_p - l_{p'}} \right) = \sum_{(\delta_k, \delta_l) \in \mathcal{D}} (\mathbf{\Pi}_N^{\delta_k} \otimes \mathbf{\Pi}_M^{\delta_l}) \end{aligned} \quad (26)$$

where the identity matrix is dropped, since it is readily proven that the diagonal elements of  $\mathbf{H}_{\text{DD}} \mathbf{V} \mathbf{H}_{\text{DD}}^{\text{H}}$  are positive. Here,  $\delta_k = k_p - k_{p'}$ ,  $\delta_l = l_p - l_{p'}$  for  $p, p' = 1, \dots, P$ , and  $\mathcal{D}$  denotes the set of pairs  $(\delta_k, \delta_l)$ . We observe that if  $(\delta_k, \delta_l) \in \mathcal{D}$ , then  $(-\delta_k, -\delta_l) \in \mathcal{D}$ , which is consistent with the fact that  $\text{sp}(\mathbf{A})$  is symmetric. Further, the degree of each node is the number of nonzero off-diagonal elements in this column. Then, according to (26), all the node degrees of  $\mathbf{A}$  are equal to  $|\mathcal{D}| - 1$ . For  $p = p'$ ,  $(\delta_k, \delta_l) = (0, 0)$  which corresponds to the diagonal elements; for  $p \neq p'$ , there are at most  $\binom{P}{2}$  combinations of  $(p, p')$ , where each combination has two distinct pairs  $(\delta_k, \delta_l)$  and  $(-\delta_k, -\delta_l)$  corresponding to off-diagonal elements. Hence, It can be verified that  $|\mathcal{D}| \leq 2\binom{P}{2} + 1$ , and the maximum degree of  $\mathbf{A}$  is  $\kappa = 2\binom{P}{2} = P(P - 1)$ .

An example is presented to illustrate the sparsity patterns of  $\mathbf{H}_{\text{DD}}$  and  $\mathbf{A}$  as shown in Fig. 2. Assume there are  $P = 3$  paths with the delay indices  $[0, 1, 2]$  and Doppler indices  $[-1, 1, 1]$ , and a small OTFS frame with  $M = 4$  and  $N = 3$  is used for convenience of analysis. In Fig. 2

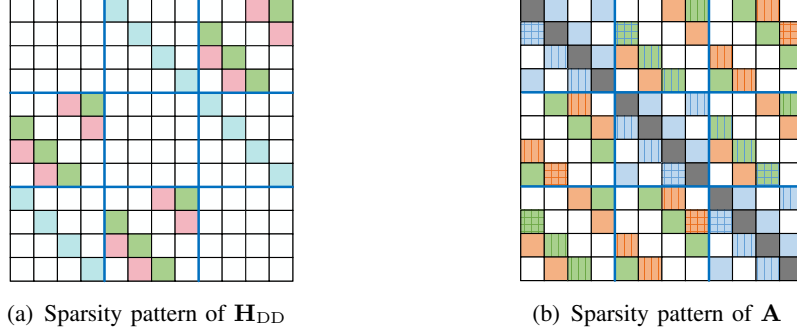


Fig. 2. An example to show the sparsity patterns of  $\mathbf{H}_{DD}$  and  $\mathbf{A}$  with  $M = 4$  and  $N = 3$ , where the delay and Doppler indices are  $[0, 1, 2]$  and  $[-1, 1, 1]$  respectively.

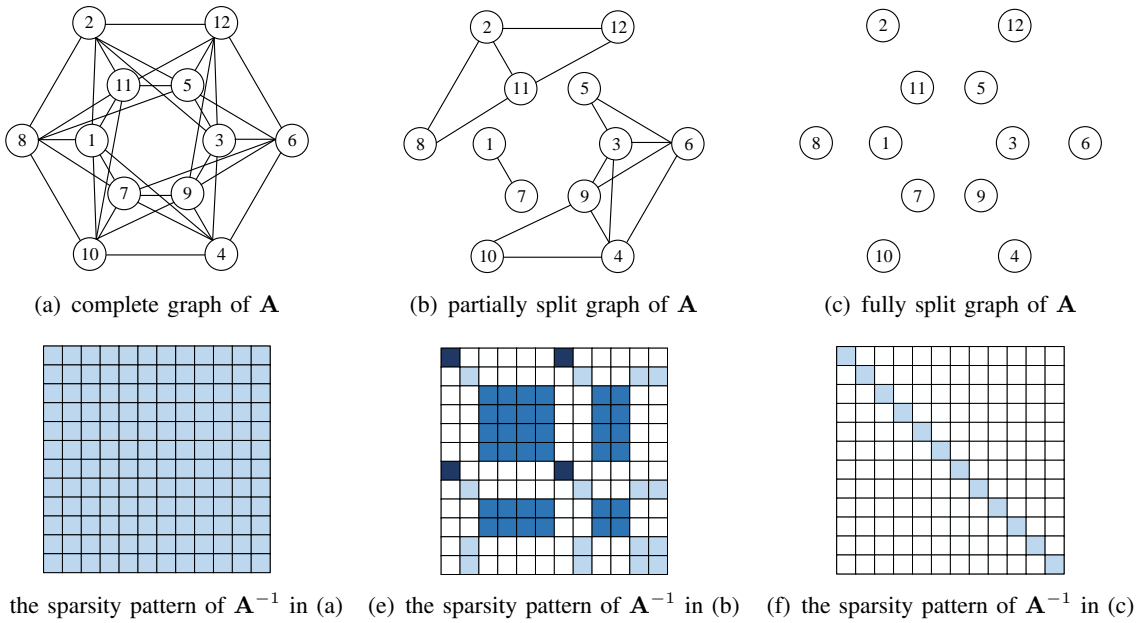


Fig. 3. Complete and split graphs of  $\mathbf{A}$  with their corresponding sparsity patterns of  $\mathbf{A}^{-1}$ , where the blank square units represent zero elements.

(a), different colors of the square units denote the nonzero elements caused by different paths, i.e.,  $\mathbf{H}_{DD}^{(p)}$  for  $p = 1, 2, 3$ . In Fig. 2 (b), different kinds of the square units denote the nonzero elements caused by different pairs in  $\mathcal{D}$ , and the square units of pairs  $(\delta_k, \delta_l)$  and  $(-\delta_k, -\delta_l)$  share the same color but differ in texture. The graph of sparse matrix  $\mathbf{A}$  in Fig. 2 is shown in Fig. 3 (a). Obviously, the nodes are connected intricately where each node has degree  $D = 6$ . The resultant  $\mathbf{A}^{-1}$  turns out to be a dense matrix whose sparsity pattern is shown in Fig. 3 (d), and each node of  $\mathbf{A}^{-1}$  has degree  $D = MN - 1$ , i.e.,  $F_\varphi(MN - 2) = 0$  and  $F_\varphi(MN - 1) = 1$ . This is the worst case that needs to be avoided.

Here, we give a special case to illustrate the effect of the guidelines. As shown in Fig. 3 (b),

after eliminating all the trivial edges and isolating all the nodes with small degree, the graph is split into three separate subgraphs. In this way,  $\mathbf{A}^{-1}$  can be derived by computing the inverse of these subgraphs individually. In Fig. 3 (e), we use different color shades to illustrate the inverse of these subgraphs. Obviously, the sparsity level of  $\mathbf{A}^{-1}$  is enhanced and thus can be derived with less complexity. As will be shown shortly, even if the graph is not ideally split into several disconnected subgraphs, the complexity can be significantly reduced with the help of the guidelines. In an extreme case, if all the nodes are fully disconnected,  $\mathbf{A}$  is perfectly reduced to a diagonal matrix whose graph is exhibited in Fig. 3 (c), and the sparsity pattern of  $\mathbf{A}^{-1}$  is also diagonal as shown in Fig. 3 (f). This is the best case, where  $F_\varphi(0) = 1$  and  $\mathbf{A}^{-1}$  can be directly obtained with complexity  $\mathcal{O}(MN)$ .

As illustrated in the example,  $\mathbf{A}$  can be computed with much less complexity after applying these two guidelines. When  $E_b/N_0$  is low,  $\mathbf{A}$  is dominated by the second term  $N_0\mathbf{I}$ , so that the diagonal elements of  $\mathbf{A}$  have much larger magnitude than the off-diagonal elements. Hence, after sparsifying  $\mathbf{A}$  according to the guidelines, most off-diagonal elements can be eliminated. Unfortunately, at high  $E_b/N_0$  the off-diagonal elements tend to have the same order of magnitude as the diagonal elements. In this case, we should avoid computing  $\mathbf{A}^{-1}$  directly. Nevertheless, with the help of the decoder, the *a priori* information is highly reliable at the second iteration, so that the updated variances are close to zero, which diminish the impact of the first term  $\mathbf{H}_{\text{DD}}\mathbf{V}\mathbf{H}_{\text{DD}}^{\text{H}}$  on  $\mathbf{A}$ . As a result, the second term  $N_0\mathbf{I}$  dominates again and the guidelines can be utilized to sparsify  $\mathbf{A}$ . In summary, reducing the complexity of MMSE estimation can be decomposed into two subproblems. The first subproblem is to perform MMSE estimation without deriving  $\mathbf{A}^{-1}$  directly at the initial iteration when the covariance matrix  $\mathbf{A}$  can hardly be sparsified by the guidelines; the second one is to derive  $\mathbf{A}^{-1}$  at the subsequent iterations when  $\mathbf{A}$  has been sparsified according to the proposed guidelines.

## V. LOW-COMPLEXITY ALGORITHMS FOR MMSE ESTIMATION

In this section, we present two low-complexity algorithms to compute  $\mathbf{A}^{-1}$ , where one of them is used at the initial outer iteration and the other is applied at the subsequent iterations. The former is the GMRES algorithm by converting the problem of computing  $\mathbf{A}^{-1}$  into solving the equivalent sparse linear systems, while the latter is the FSPAI algorithm to derive an approximation of  $\mathbf{A}^{-1}$  with the help of the proposed sparsification guidelines.

### A. GMRES at the Initial Outer Iteration

Due to the lack of *a priori* information at the initial iteration, we have  $\mathbf{A} = \mathbf{H}_{\text{DD}}\mathbf{H}_{\text{DD}}^{\text{H}} + N_0\mathbf{I}$ . In this case, the off-diagonal elements of  $\mathbf{A}$  has a comparable order to that of the diagonal elements, so that the sparsity level of  $\mathbf{A}^{-1}$  can only be slightly enhanced. Hence, directly deriving  $\mathbf{A}^{-1}$  is not a good option. As described in Section III,  $\mathbf{A}^{-1}$  is needed in two places when MMSE estimation is performed, namely  $\mathbf{A}^{-1}(\mathbf{y} - \mathbf{H}_{\text{DD}}\mathbf{m})$  of (19) and  $\xi_n = \mathbf{h}_n^{\text{H}}\mathbf{A}^{-1}\mathbf{h}_n$  of (19) and (22), which are discussed separately in the following.

With regard to the former, we observe that  $\mathbf{A}^{-1}(\mathbf{y} - \mathbf{H}_{\text{DD}}\mathbf{m})$  is a common part of all the estimated symbol  $\hat{x}_n$ , where  $\mathbf{A}^{-1}(\mathbf{y} - \mathbf{H}_{\text{DD}}\mathbf{m}) = \mathbf{A}^{-1}\mathbf{y}$  since  $\mathbf{m}$  is of all zeros at the initial iteration. Therefore, for all  $\hat{x}_n$ 's, we can solve only one equivalent sparse linear system  $\mathbf{A}\mathbf{f}_1 = \mathbf{y}$ , where  $\mathbf{f}_1$  is the vector of unknowns, and avoid directly computing  $\mathbf{A}^{-1}$ .

As for computing  $\xi_n$ , all  $\xi_n$ 's for  $n = 1, \dots, MN$  are almost the same for a given  $\mathbf{H}_{\text{DD}}$  as shown in Fig. 4, where  $v_\xi = \mathbb{E}\{|\xi_n - \frac{1}{MN} \sum_{n=1}^{MN} \xi_n|^2\}$  is the variance of  $\xi_n$ . It is found that  $v_\xi$  converges to zero when  $E_b/N_0$  is extremely low or high. According to  $\xi_n = \mathbf{h}_n^{\text{H}}\mathbf{A}^{-1}\mathbf{h}_n$ ,  $\xi_n$  is actually the diagonal element of  $\mathbf{B} = \mathbf{H}_{\text{DD}}^{\text{H}}(\mathbf{H}_{\text{DD}}\mathbf{H}_{\text{DD}}^{\text{H}} + N_0\mathbf{I})^{-1}\mathbf{H}_{\text{DD}}$ . If  $E_b/N_0$  is low enough,  $\mathbf{B}$  can be approximated as  $\mathbf{B} \approx N_0^{-1}\mathbf{H}_{\text{DD}}^{\text{H}}\mathbf{H}_{\text{DD}}$  whose diagonal elements are all equal to  $N_0^{-1} \sum_{p=1}^P |h_p|^2$  and  $v_\xi \approx 0$ . If  $E_b/N_0$  is sufficiently high, we have  $\mathbf{B} \approx \mathbf{H}_{\text{DD}}^{\text{H}}(\mathbf{H}_{\text{DD}}\mathbf{H}_{\text{DD}}^{\text{H}})^{-1}\mathbf{H}_{\text{DD}} = \mathbf{I}$  and thus  $v_\xi \approx 0$ . Moreover, as observed in Fig. 4, even the maximum value of  $v_\xi$  is smaller than  $10^{-5}$ . Hence, it is reasonable to assume that  $\xi_n$ 's are the same for  $n = 1, \dots, MN$ . Then, deriving  $\xi_n$ 's can be converted to solving another sparse linear system  $\mathbf{A}\mathbf{f}_2 = \mathbf{h}_n$  for any  $n$ , where  $\mathbf{f}_2 = \mathbf{A}^{-1}\mathbf{h}_n$  is another vector of unknowns. Thereafter, little computation is required to obtain  $\xi_n$  through  $\xi_n = \mathbf{h}_n^{\text{H}}\mathbf{f}_2$ , since  $\mathbf{h}_n$  is sparse with only  $P$  nonzero elements. In this way, we can solve two equivalent sparse linear systems at the initial iteration instead of directly calculating  $\mathbf{A}^{-1}$ .

We use an iterative algorithm called GMRES to solve the sparse linear systems, since GMRES has no requirements for the coefficient matrix  $\mathbf{A}$  of a linear system  $\mathbf{A}\mathbf{f} = \mathbf{b}$ . Besides, GMRES takes less computation than some other candidate iterative algorithms, such as the Generalized Conjugate Residual (GCR) algorithm [20]. More importantly, the global convergence of GMRES applied in our system can be guaranteed with limited iterations (as will be presented in Section VI-A). Note that if MMSE estimation is only performed once without subsequent outer iterations, the iterative equalizer is reduced to a conventional LMMSE equalizer. Hence, GMRES can be readily extended to any other systems with LMMSE equalizer. Next, we will briefly introduce

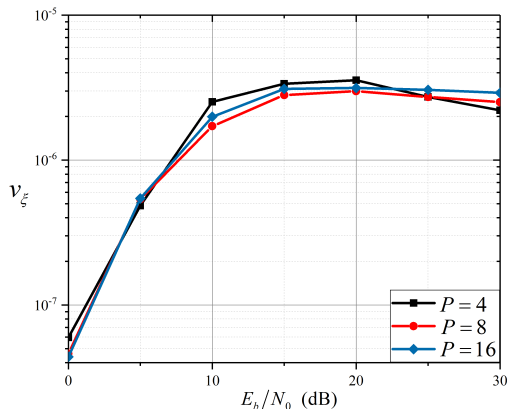


Fig. 4. The variance of  $\xi_n$  versus  $E_b/N_0$ , where  $M = 64$ ,  $N = 32$  and  $P = 4, 8, 16$ . At each  $E_b/N_0$  we average over 1000 channel realizations.

how to apply GMRES at the initial iteration.

For a linear system  $\mathbf{A}\mathbf{f} = \mathbf{b}$ , GMRES uses an arbitrary initial guess  $\mathbf{f}_0$ , e.g., a zero vector, to extract an approximate solution  $\mathbf{f}_j = \mathbf{f}_0 + \Delta\mathbf{f}_j$  iteratively, where  $\Delta\mathbf{f}_j$  is obtained from a subspace  $\mathcal{K}_j \in \mathbb{C}^j$  to minimize the current residual norm  $\|\mathbf{r}_j\| \triangleq \|\mathbf{b} - \mathbf{A}\mathbf{f}_j\|$  [20]. Here,  $\mathcal{K}_j$  is the  $j$ -th Krylov subspace  $\mathcal{K}_j = \text{span}\{\mathbf{r}_0, \mathbf{A}\mathbf{r}_0, \dots, \mathbf{A}^{j-1}\mathbf{r}_0\}$  with the initial residual  $\mathbf{r}_0 \triangleq \mathbf{b} - \mathbf{A}\mathbf{f}_0$ . For convenience, we set the norm  $\|\mathbf{r}_0\| = \rho$ . Then the least-squares (LS) problem can be written as

$$\min_{\Delta\mathbf{f}_j \in \mathcal{K}_j} \|\mathbf{b} - \mathbf{A}(\mathbf{f}_0 + \Delta\mathbf{f}_j)\| = \min_{\Delta\mathbf{f}_j \in \mathcal{K}_j} \|\mathbf{r}_0 - \mathbf{A}\Delta\mathbf{f}_j\|. \quad (27)$$

When the residual norm is smaller than a drop tolerance  $\epsilon_g$ , the algorithm stops. Otherwise, the subspace needs to be expanded to  $\mathcal{K}_{j+1}$ , from which the approximate solution is updated to  $\mathbf{f}_{j+1}$  to derive a more precise solution. This update process is an inner iteration.

However, with the expansion of the subspace, the computational cost increases exponentially. Hence, we let  $j_m$  be the maximum dimension of the Krylov subspace. After the  $j_m$ -th inner iteration, if the drop tolerance  $\epsilon_g$  is still not reached, then compute the current approximate solution  $\mathbf{f}_{j_m}$  and restart GMRES with a new initial guess  $\mathbf{f}'_0 = \mathbf{f}_{j_m}$ . These  $j_m$  inner iterations is called a restart cycle, and the restarting step can control the overall complexity of GMRES.

Considering that the LS problem of (27) dominates the complexity, we can reduce (27) into a smaller problem [21]. We first use the modified Gram-Schmidt algorithm to yield the  $\ell_2$ -orthonormal basis  $\{\mathbf{p}_1, \mathbf{p}_2, \dots, \mathbf{p}_j\}$  of  $\mathcal{K}_j$  as summarized in lines 4-8 of Algorithm 1 [22], where  $\mathbf{p}_i \in \mathbb{C}^{MN}$  for  $i = 1, \dots, j$ . Since  $\Delta\mathbf{f}_j$  is derived from  $\mathcal{K}_j$ ,  $\Delta\mathbf{f}_j$  can be denoted by a linear combination of the orthonormal basis as  $\Delta\mathbf{f}_j = \mathbf{P}_j\mathbf{k}_j$  where  $\mathbf{P}_j = [\mathbf{p}_1, \mathbf{p}_2, \dots, \mathbf{p}_j]$  and  $\mathbf{k}_j \in \mathbb{C}^j$ . Then, from the modified Gram-Schmidt algorithm,  $\mathbf{A}\mathbf{p}_j$  is rewritten as



$$\mathbf{A}\mathbf{p}_j = \sum_{i=1}^{j+1} t_{i,j} \mathbf{p}_i, \quad (28)$$

where  $t_{i,j} = (\mathbf{A}\mathbf{p}_j, \mathbf{p}_i)$ . Therefore, we have  $\mathbf{A}\mathbf{P}_j = [\mathbf{A}\mathbf{p}_1, \dots, \mathbf{A}\mathbf{p}_j] = \mathbf{P}_{j+1} \mathbf{T}_j$  where  $\mathbf{T}_j$  is an upper Hessenberg matrix

$$\mathbf{T}_j = \begin{bmatrix} t_{1,1} & \cdots & t_{1,j} \\ t_{2,1} & \cdots & t_{2,j} \\ & \ddots & \vdots \\ & & t_{j+1,j} \end{bmatrix}_{(j+1) \times j}.$$

By substituting  $\Delta \mathbf{f}_j = \mathbf{P}_j \mathbf{k}_j$  into (27), the LS problem reduces to

$$\min_{\mathbf{k}_j} \|\rho \mathbf{p}_1 - \mathbf{A}\mathbf{P}_j \mathbf{k}_j\| = \min_{\mathbf{k}_j} \left\| \rho \mathbf{P}_{j+1} \mathbf{e}_1^{(j)} - \mathbf{P}_{j+1} \mathbf{T}_j \mathbf{k}_j \right\| = \min_{\mathbf{k}_j} \left\| \rho \mathbf{e}_1^{(j)} - \mathbf{T}_j \mathbf{k}_j \right\|, \quad (29)$$

where  $\mathbf{e}_i^{(j)}$  is the  $i$ -th column of the identity matrix  $\mathbf{I}_{j+1}$ . The computation of solving (29) is trivial since  $\mathbf{T}_j$  is a  $j \times (j+1)$  matrix, where  $j$  has a maximum value  $j_m$  and is generally much smaller than  $MN$ .

In GMRES, whether to start the next iteration of GMRES is determined by the residual norm from (29). To avoid solving (29) repeatedly, we can solve the LS problem of (29) by transforming  $\mathbf{T}_j$  into an upper triangular matrix  $\mathbf{U}_j$  column by column using the rotation matrix

$$\Psi_i^{(j)} = \begin{bmatrix} 1 & & & & & \\ & \ddots & & & & \\ & & \varsigma_i & \vartheta_i & & \\ & & -\vartheta_i & \varsigma_i & & \\ & & & & \ddots & \\ & & & & & 1 \end{bmatrix}_{(j+1) \times (j+1)}, \quad (30)$$

where  $\varsigma_i = t_{i,i}/(t_{i,i}^2 + t_{i+1,i}^2)^{1/2}$  and  $\vartheta_i = t_{i+1,i}/(t_{i,i}^2 + t_{i+1,i}^2)^{1/2}$  are in the  $i$ -th and  $(i+1)$ -th rows for  $i = 1, 2, \dots, j$ . Using  $\Psi_i^{(j)}$ , we derive the upper triangular matrix as

$$\mathbf{U}_j = \Psi_j^{(j)} \dots \Psi_2^{(j)} \Psi_1^{(j)} \mathbf{T}_j = \Xi_j \mathbf{T}_j = \begin{bmatrix} u_{1,1} & \cdots & u_{1,j} \\ & \ddots & \vdots \\ & & u_{j,j} \\ & & & 0 \end{bmatrix}, \quad (31)$$

where  $\Xi_j = \Psi_j^{(j)} \dots \Psi_2^{(j)} \Psi_1^{(j)}$ . Then, the LS problem is rewritten as

$$\min_{\mathbf{k}_j} \left\| \Xi_j (\rho \mathbf{e}_1^{(j)} - \mathbf{T}_j \mathbf{k}_j) \right\| = \min_{\mathbf{k}_j} \|\mathbf{w}_j - \mathbf{U}_j \mathbf{k}_j\|, \quad (32)$$

where  $\mathbf{w}_j = \rho \Xi_j \mathbf{e}_1^{(j)}$ . Now we can easily solve the LS problem using backward substitution. Since the last row of  $\mathbf{U}_j$  is of all zeros, all rows except the last one in  $\mathbf{w}_j - \mathbf{U}_j \mathbf{k}_j$  can be canceled out by choosing  $\mathbf{k}_j$ . Thus, the current residual is readily derived from the last element of  $\mathbf{w}_j$  without any additional computation, i.e.,  $\|\mathbf{r}_j\| = |\mathbf{w}_j(j+1)|$ . The LS problem is solved only when the current restart cycle finishes or the algorithm stops.

The complete algorithm is summarized in Algorithm 1. Initially, set  $\mathbf{U}$  as a  $(j_m + 1) \times j_m$  zero

---

**Algorithm 1:** Restarted GMRES
 

---

```

1 Initialization:  $\mathbf{r}_0 = \mathbf{b} - \mathbf{A}\mathbf{f}_0$ ,  $\rho = \|\mathbf{r}_0\|$ ,  $\mathbf{p}_1 = \mathbf{r}_0/\rho$ ,
2            $\mathbf{w} = \rho\mathbf{e}_1^{(j_m)}$ ,  $\mathbf{T}$  and  $\mathbf{U}$  are  $(j_m + 1) \times j_m$  zero matrix ;
3 for  $j = 1$  to  $j_m$  do
4    $\tilde{\mathbf{p}}_{j+1} = \mathbf{A}\mathbf{p}_j$ ;
5   for  $i = 1$  to  $j$  do
6      $t_{i,j} = (\mathbf{A}\mathbf{p}_j, \mathbf{p}_i)$ ,  $\tilde{\mathbf{p}}_{j+1} \leftarrow \tilde{\mathbf{p}}_{j+1} - t_{i,j}\mathbf{p}_i$ .
7   end
8    $t_{j+1,j} = \|\tilde{\mathbf{p}}_{j+1}\|$ ,  $\mathbf{p}_{j+1} = \tilde{\mathbf{p}}_{j+1}/t_{j+1,j}$ ;
9    $\mathbf{T}(1:j+1, j) \leftarrow [t_{1,j}, t_{2,j}, \dots, t_{j+1,j}]^T$ ;
10  Compute  $\Psi_i^{(j_m)}$ , for  $i = 1, 2, \dots, j$ ;
11   $\mathbf{U}(:, j) \leftarrow \Psi_j^{(j_m)} \dots \Psi_2^{(j_m)} \Psi_1^{(j_m)} \mathbf{T}(:, j)$ ,  $\mathbf{w} \leftarrow \Psi_j^{(j_m)} \mathbf{w}$ ;
12  if  $|\mathbf{w}(j+1)| < \epsilon_g$  then
13    Solve: the LS problem  $\min_{\mathbf{k}_j} \|\mathbf{w}(1:j+1) - \mathbf{U}(1:j+1, 1:j)\mathbf{k}_j\|$ ,
14     $\mathbf{f}_j = \mathbf{f}_0 + \mathbf{P}_j\mathbf{k}_j$ ;
15    Stop
16  end
17 Solve: the LS problem  $\min_{\mathbf{k}_{j_m}} \|\mathbf{w} - \mathbf{U}\mathbf{k}_{j_m}\|$ ,  $\mathbf{f}_{j_m} = \mathbf{f}_0 + \mathbf{P}_{j_m}\mathbf{k}_{j_m}$ ;
18 Restart:  $\mathbf{r}_0 = \mathbf{b} - \mathbf{A}\mathbf{f}_{j_m}$ ,  $\rho = \|\mathbf{r}_0\|$ ,  $\mathbf{p}_1 = \mathbf{r}_0/\rho$ ,
19            $\mathbf{w} = \rho\mathbf{e}_1^{(j_m)}$ ,  $\mathbf{T}$  and  $\mathbf{U}$  are  $(j_m + 1) \times j_m$  zero matrix;
20 Go to Line 3.

```

---

matrix, and transform  $\mathbf{T}_{j_m}$  to  $\mathbf{U}_{j_m}$  progressively in  $j_m$  inner iterations. At the  $j$ -th inner iteration ( $j = 1, \dots, j_m$ ), we use the modified Gram-Schmidt algorithm and obtain  $\{t_{1,j}, t_{2,j}, \dots, t_{j+1,j}\}$  as shown in lines 4-8. The new column  $[t_{1,j}, t_{2,j}, \dots, t_{j+1,j}]^T$  is first multiplied by all the previous  $\Psi_i^{(j_m)}$  for  $i = 1, 2, \dots, j-1$ , since the previous rotation matrices also affect this newly produced column. Then,  $\Psi_j^{(j_m)}$  is used to eliminate  $t_{j+1,j}$ . Meanwhile,  $\mathbf{w}$  is multiplied by  $\Psi_j^{(j_m)}$  according to (32). These steps are shown in lines 10-11. If the current residual  $|\mathbf{w}_j(j+1)| > \epsilon_g$ , another iteration is performed. At the end of a restart cycle, if norm  $\|\mathbf{r}_{j_m}\|$  is still larger than  $\epsilon_g$ , then restart the algorithm and go to line 3.

### B. FSPAI at the Subsequent Outer Iterations

After the first outer iteration, we have obtained new means and variances, which serve as the *a priori* information to start the next outer iteration. However, since the variances matrix  $\mathbf{V}$  is no longer an identity matrix,  $\xi_n$ 's have completely different values for  $n = 1, \dots, MN$ . As a result, GMRES needs to be used  $MN$  times per outer iteration to derive each  $\xi_n$ , which is not acceptable for the subsequent outer iterations. However, with the help of the decoder,

most *a priori* information of the estimator is reliable enough, so that the corresponding new variances of the estimated symbols approach zero. Hence, the second term  $N_0\mathbf{I}$  of  $\mathbf{A}$  dominates, and the diagonal elements have much larger magnitude than other elements. By sparsifying  $\mathbf{A}$  according to the guidelines,  $\mathbf{A}$  becomes much sparser, and the sparsity level of  $\mathbf{A}^{-1}$  can be greatly enhanced. Thus, we can use the FSPA algorithm to yield a sparse approximation of  $\mathbf{A}^{-1}$ , which is inherently parallelizable and can further save the computational time.

We observe that the covariance matrix  $\mathbf{A}$  is Hermitian positive definite (HPD), since  $\mathbf{A} = \mathbf{H}_{\text{DD}}\mathbf{V}\mathbf{H}_{\text{DD}}^{\text{H}} + N_0\mathbf{I}$  is the sum of a Gram matrix and an identity matrix [23]. For an HPD matrix  $\mathbf{A} = \mathbf{L}_A^{\text{H}}\mathbf{L}_A$  with Cholesky factor  $\mathbf{L}_A$ , the inverse  $\mathbf{A}^{-1}$  can be obtained by deriving a sparse approximate Cholesky factor  $\mathbf{L}$  such that  $\mathbf{L}\mathbf{L}^{\text{H}} \approx \mathbf{A}^{-1}$ . Here,  $\mathbf{L}$  is a lower triangular matrix and can be obtained by minimizing the Frobenius norm  $\|\mathbf{L}_A\mathbf{L} - \mathbf{I}\|_F$  with respect to a prescribed sparsity pattern of  $\mathbf{L}$ , denoted by  $\text{sp}(\mathbf{L}) = \mathcal{L}$  [24]. This is equivalent to minimizing the Kaporin condition number of  $\mathbf{L}^{\text{H}}\mathbf{A}\mathbf{L}$ , which is defined as [25]

$$K = \frac{\text{tr}(\mathbf{L}^{\text{H}}\mathbf{A}\mathbf{L})}{MN \cdot \det(\mathbf{L}^{\text{H}}\mathbf{A}\mathbf{L})^{\frac{1}{MN}}}, \quad (33)$$

where  $\text{tr}(\cdot)$  and  $\det(\cdot)$  denote the trace and determinant of a matrix respectively, and  $K$  measures the quality of the sparse approximation where  $K \geq 1$ . Evidently, a more precise  $\mathbf{L}$  makes  $\mathbf{L}^{\text{H}}\mathbf{A}\mathbf{L}$  closer to  $\mathbf{I}$ , and thus  $K$  is closer to one. By minimizing  $K$ , FSPA can capture the sparsity pattern of  $\mathbf{L}$  dynamically [26]. Since the consequent  $\mathbf{L}$  is typically sparse, there is a significant reduction in complexity. As opposed to the conventional FSPA used in symmetric positive definite linear system, FSPA applied in our system should be modified to match the HPD case.

Initially, a prescribed sparsity pattern  $\text{sp}(\mathbf{L})$  is selected, e.g.,  $\text{sp}(\mathbf{L}) = \mathbf{I}$  with only diagonal elements nonzero. Let  $\mathbf{a}_k$  and  $\mathbf{l}_k$  be the  $k$ -th column of  $\mathbf{A}$  and  $\mathbf{L}$  respectively. Let  $\mathcal{C}_k$  denote the set of nonzero element indices of  $\mathbf{l}_k$  and  $\tilde{\mathcal{C}}_k = \mathcal{C}_k \setminus \{k\}$ . Then we have

$$\begin{aligned} K &= \frac{\text{tr}(\mathbf{L}^{\text{H}}\mathbf{A}\mathbf{L})}{MN \cdot \det(\mathbf{L}^{\text{H}}\mathbf{A}\mathbf{L})^{\frac{1}{MN}}} = \frac{\sum_{k=1}^{MN} \mathbf{l}_k^{\text{H}}\mathbf{A}\mathbf{l}_k}{MN \cdot [\det(\mathbf{L}^{\text{H}})\det(\mathbf{A})\det(\mathbf{L})]^{\frac{1}{MN}}} \\ &= \frac{\sum_{k=1}^{MN} \left[ l_{kk}^2 a_{kk} + 2l_{kk} \text{Re}\{\mathbf{l}_k(\tilde{\mathcal{C}}_k)^{\text{H}}\mathbf{a}_k(\tilde{\mathcal{C}}_k)\} + \mathbf{l}_k(\tilde{\mathcal{C}}_k)^{\text{H}}\mathbf{A}(\tilde{\mathcal{C}}_k, \tilde{\mathcal{C}}_k)\mathbf{l}_k(\tilde{\mathcal{C}}_k) \right]}{MN \cdot \det(\mathbf{A})^{\frac{1}{MN}} \left( \prod_{k=1}^{MN} l_{kk}^{\frac{2}{MN}} \right)}, \end{aligned} \quad (34)$$

where  $l_{kk} = \mathbf{L}(k, k) \in \mathbb{R}^+$  and  $a_{kk} = \mathbf{A}(k, k) \in \mathbb{R}^+$ . For each column,  $l_{kk}$  and  $\mathbf{l}_k(\tilde{\mathcal{C}}_k)$  are obtained to minimize  $K$ . To do so, we let  $\partial K / \partial l_{kk} = 0$  and  $\partial K / \partial \mathbf{l}_k(\tilde{\mathcal{C}}_k) = 0$ , and then

$$\mathbf{q}_k = \mathbf{A}(\tilde{\mathcal{C}}_k, \tilde{\mathcal{C}}_k)^{-1} \mathbf{a}_k(\tilde{\mathcal{C}}_k), \quad (35a)$$

$$l_{kk} = \left( a_{kk} - \mathbf{a}_k(\tilde{\mathcal{C}}_k)^H \mathbf{q}_k \right)^{-\frac{1}{2}}, \quad (35b)$$

$$\mathbf{l}_k(\tilde{\mathcal{C}}_k) = -l_{kk} \mathbf{q}_k. \quad (35c)$$

Since  $l_{kk}$  and  $\mathbf{l}_k(\tilde{\mathcal{C}}_k)$  are independently computed for each column,  $\mathbf{L}$  can be obtained column by column in parallel. Due to the parallelism, we only consider  $\mathbf{l}_k$  in the following.

FSPA iteratively improves the approximation by carefully choosing new index  $r$  and adding it to  $\mathcal{C}_k$ . This process of augmenting  $\mathcal{C}_k$  is called an inner iteration of FSPA. The improved approximation is derived as  $\mathbf{l}'_k = \mathbf{l}_k + l_{rk} \mathbf{e}_r$ , where  $\mathbf{e}_r$  denotes the  $r$ -th column of  $\mathbf{I}$  and  $r > k$ . To minimize the new Kaporin condition number  $K'_r$  for index  $r$ , we need to solve [19]

$$\begin{aligned} \min_{l_{rk}} K'_r &= \min_{l_{rk}} \frac{\text{tr} \left( (\mathbf{L} + l_{rk} \mathbf{e}_r \mathbf{e}_r^H)^H \mathbf{A} (\mathbf{L} + l_{rk} \mathbf{e}_r \mathbf{e}_r^H) \right)}{MN \cdot \det \left( (\mathbf{L}^H + l_{rk}^* \mathbf{e}_r \mathbf{e}_r^H) \mathbf{A} (\mathbf{L} + l_{rk} \mathbf{e}_r \mathbf{e}_r^H) \right)^{\frac{1}{MN}}} \\ &= \min_{l_{rk}} \frac{\text{tr}(\mathbf{L}^H \mathbf{A} \mathbf{L}) + 2\text{Re}\{l_{rk}^* \mathbf{a}_r^H \mathbf{l}_k\} + a_{rr} |l_{rk}|^2}{MN \cdot \det(\mathbf{A})^{\frac{1}{MN}} \left( \prod_{k=1}^{MN} l_{kk}^{\frac{2}{MN}} \right)}, \end{aligned} \quad (36)$$

which can be derived by letting the derivative  $\partial K'_r / \partial l_{rk} = 0$ . Then, we have

$$l_{rk} = -\frac{\mathbf{a}_r^H \mathbf{l}_k}{a_{rr}} = -\frac{\mathbf{a}_r(\mathcal{C}_k)^H \mathbf{l}_k(\mathcal{C}_k)}{a_{rr}},$$

where the sparsity of  $\mathbf{l}_k$  is taken into account, and thus trivial computation is entailed to derive  $l_{rk}$ . With  $l_{rk}$ , the minimum of  $K'_r$  for index  $r$  is

$$\min_{l_{rk}} K'_r = \left( 1 - \frac{\eta_{rk}}{MN} K \right), \quad (37)$$

where  $\eta_{rk} = |\mathbf{a}_r^H \mathbf{l}_k|^2 / a_{rr}$  measures the reduction in Kaporin condition number by adding the new index  $r$ . Due to the sparsity of  $\mathbf{A}$ , only a small fraction of indices  $r$  satisfy  $\mathbf{a}_r(\mathcal{C}_k)^H \mathbf{l}_k(\mathcal{C}_k) \neq 0$ , such that the approximation can be improved as shown in (37). Resorting to the graph of  $\mathbf{A}$  in Section IV, we can readily find these indices that are defined as  $\hat{\mathcal{C}}_k = \{r : r > k \text{ and } \mathbf{a}_r(\mathcal{C}_k)^H \mathbf{l}_k(\mathcal{C}_k) \neq 0\} \setminus \mathcal{C}_k$ . Thereafter, we can add one or more indices from  $\hat{\mathcal{C}}_k$  with the largest  $\eta_{rk}$  to  $\mathcal{C}_k$ , and obtain augmented indices sets  $\mathcal{C}'_k$  and  $\tilde{\mathcal{C}}'_k = \mathcal{C}'_k \setminus \{k\}$ . Then a more precise solution  $\mathbf{l}'_k$  is derived according to (35). Note that the complexity of FSPA is dominated by computing the inverse in (35a). Hence, the cardinality of  $\tilde{\mathcal{C}}_k$  should not exceed a certain value  $\zeta$  in light of complexity constraints. Generally,  $\zeta = P$  is sufficient to derive a precise enough solution. The algorithm keeps iterating until  $|\tilde{\mathcal{C}}_k| > \zeta$  or the maximum of  $\eta_{rk}$  is smaller than a well-chosen tolerance  $\epsilon_f$ .

The entire FSPA is summarized in Algorithm 2, where the initial sparsity pattern of  $\mathbf{L}$  is

**Algorithm 2:** FSPAI

---

```

1 Initialization:  $\text{sp}(L) = \mathbf{I}$ ,  $\epsilon_f \geq 0$ ,  $\zeta \geq 0$  ;
2 for  $k = 1$  to  $MN$  do
3    $\mathcal{C}_k \leftarrow \{k\}$ ,  $\tilde{\mathcal{C}}_k \leftarrow \emptyset$ ,  $l_{kk} \leftarrow \sqrt{a_{kk}}$ ;
4   while  $|\tilde{\mathcal{C}}_k| < \zeta$  do
5      $\hat{\mathcal{C}}_k = \{r : r > k \text{ and } \mathbf{a}_r(\mathcal{C}_k)^H \mathbf{l}_r(\mathcal{C}_k) \neq 0\} \setminus \mathcal{C}_k$ ;
6      $\eta_{rk} \leftarrow |\mathbf{a}_r(\mathcal{C}_k)^H \mathbf{l}_r(\mathcal{C}_k)|^2 / a_{rr}$ , for each  $r \in \hat{\mathcal{C}}_k$ ;
7      $\eta_{\max} = \max_{r \in \hat{\mathcal{C}}_k} \eta_{rk}$  ;
8     if  $\eta_{\max} < \epsilon_f$  then
9       | Stop.
10    end
11     $\mathcal{C}_k \leftarrow \mathcal{C}_k \cup \{r : \eta_{rk} = \eta_{\max}\}$ ,  $\tilde{\mathcal{C}}_k \leftarrow \mathcal{C}_k \setminus \{k\}$ ;
12     $\mathbf{q}_k \leftarrow \mathbf{A}(\tilde{\mathcal{C}}_k, \tilde{\mathcal{C}}_k)^{-1} \mathbf{a}_k(\tilde{\mathcal{C}}_k)$ ;
13     $l_{kk} \leftarrow (a_{kk} - \mathbf{a}_k(\tilde{\mathcal{C}}_k)^H \mathbf{q}_k)^{-\frac{1}{2}}$ ;
14     $\mathbf{l}_k(\tilde{\mathcal{C}}_k) \leftarrow -l_{kk} \mathbf{q}_k$ .
15  end
16 end

```

---

set to be diagonal, and for each column, only one single index with the largest  $\zeta_{rk}$  is added to  $\mathcal{C}_k$  during each index update. Other initial sparsity patterns and index update strategies can be readily applied with trivial modifications.

## VI. THEORETICAL ANALYSIS

## A. Convergence Analysis

In what follows, full GMRES (without restarting) used in the MMSE estimator is proven to globally converge, and the upper bound of its convergence rate is derived. Then we prove that for restarted GMRES,  $j_m$  can be chosen arbitrarily without losing the global convergence.

For full GMRES, considering the definition of Krylov subspace, the residual norm at the  $j$ -th inner iteration for  $j \geq 1$  can be written as

$$\|\mathbf{r}_j\| = \min_{\Delta \mathbf{f}_j \in \mathcal{K}_j} \|\mathbf{r}_0 - \mathbf{A} \Delta \mathbf{f}_j\| = \min_{p_j \in \mathcal{P}_j} \|p_j(\mathbf{A}) \mathbf{r}_0\|, \quad (38)$$

where  $\mathcal{P}_j$  denotes the set of polynomials satisfying  $p_j(\mathbf{A}) = \sum_{i=0}^j \alpha_i \mathbf{A}^i$  and  $\alpha_0 = 1$  [27]. Since  $\mathbf{A}$  is Hermitian,  $\mathbf{A}$  can be diagonalized as  $\mathbf{A} = \mathbf{U}_A \mathbf{\Lambda} \mathbf{U}_A^H$  with unitary matrix  $\mathbf{U}_A$  and diagonal matrix  $\mathbf{\Lambda}$ . As proven in [20], for a diagonalizable  $\mathbf{A}$ , the relative residual norm satisfies [20]

$$\frac{\|\mathbf{r}_j\|}{\|\mathbf{r}_0\|} \leq \min_{p_j \in \mathcal{P}_j} \max_{\lambda_A \in \text{eig}(\mathbf{A})} |p_j(\lambda_A)|, \quad (39)$$

where  $\text{eig}(\mathbf{A})$  denotes the spectrum of  $\mathbf{A}$  and  $\lambda_A$  represents the eigenvalues of  $\mathbf{A}$ . Since  $\mathbf{A}$  is HPD, we have  $\lambda_A \in \mathbb{R}^+$  and (39) can be bounded as [28]

$$\frac{\|\mathbf{r}_j\|}{\|\mathbf{r}_0\|} \leq \min_{p_j \in \mathcal{P}_j} \max_{\lambda \in [\lambda_{\min}, \lambda_{\max}]} |p_j(\lambda)| = [T_j(\varrho)]^{-1}, \quad (40)$$

where  $[\lambda_{\min}, \lambda_{\max}]$  is an interval in  $\mathbb{R}$  with  $\lambda_{\min}$  and  $\lambda_{\max}$  denoting the minimal and maximal eigenvalues of  $\mathbf{A}$  respectively, and  $\varrho = (\lambda_{\max} + \lambda_{\min})/(\lambda_{\max} - \lambda_{\min})$  satisfying  $\varrho \geq 1$ . Here,  $T_j$  is the Chebyshev polynomial of degree  $j$  of the first kind as

$$T_j(\varrho) = \frac{1}{2} \left[ \left( \varrho + \sqrt{\varrho^2 - 1} \right)^j + \left( \varrho - \sqrt{\varrho^2 - 1} \right)^j \right]. \quad (41)$$

If  $\lambda_{\max} = \lambda_{\min} \equiv \lambda$ , i.e.,  $\varrho = 1$ , then  $\mathbf{A} = \lambda \mathbf{U}_A \mathbf{I} \mathbf{U}_A^H = \lambda \mathbf{I}$ . This happens if and only if  $\mathbf{H}_{\text{DD}}$  is diagonal, i.e.,  $P = 1$  with  $\tau = 0$  and  $\nu = 0$ . This indicates that there is only one time-invariant path, which conflicts with the assumption of the doubly selective channel, and thus  $\varrho > 1$ .

**Theorem 1.** *Full GMRES applied to MMSE estimation globally converges with a convergence rate at least  $[T_j(\varrho)]^{-1}$ .*

*Proof.* Applying Jessen's inequality to the concave function  $x^n$  yields the inequality  $(x_1^n + x_2^n)/2 \geq [(x_1 + x_2)/2]^n$ . Then the Chebyshev polynomial in (41) satisfies

$$[T_j(\varrho)]^{-1} \leq \left( (\varrho + \sqrt{\varrho^2 - 1} + \varrho - \sqrt{\varrho^2 - 1})/2 \right)^{-j} = \varrho^{-j} < 1, \quad (42)$$

for any  $j \geq 1$ . Thus, according to (40), the relative residual norm decreases monotonically with  $j$ , and thus the GMRES algorithm converges at least as rapidly as  $[T_j(\varrho)]^{-1}$ .  $\square$

From Theorem 1, we can infer the relation between  $E_b/N_0$  and the convergence rate as follows.

**Corollary 1.** *The convergence rate of full GMRES decreases with  $E_b/N_0$ .*

*Proof.* For  $\mathbf{A} = \mathbf{H}_{\text{DD}} \mathbf{V} \mathbf{H}_{\text{DD}}^H + N_0 \mathbf{I}$ , we have  $\lambda_A = \bar{\lambda} + N_0$ , where  $\bar{\lambda}$  denotes the eigenvalues of  $\mathbf{H}_{\text{DD}} \mathbf{V} \mathbf{H}_{\text{DD}}^H$ . Then  $\varrho$  can be rewritten as

$$\varrho = \frac{\lambda_{\max} + \lambda_{\min}}{\lambda_{\max} - \lambda_{\min}} = \frac{\bar{\lambda}_{\max} + \bar{\lambda}_{\min} + 2N_0}{\bar{\lambda}_{\max} - \bar{\lambda}_{\min}}. \quad (43)$$

Thus, for a specific channel realization  $\mathbf{H}_{\text{DD}}$ ,  $\varrho$  is completely governed by  $N_0$ . Furthermore, it can be easily proven that  $T_j(\varrho)$  monotonically increases with  $\varrho$  for  $\varrho > 1$ . Since the energy of transmitted symbols is normalized, the increase of  $E_b/N_0$  is equivalent to the decrease of  $N_0$ . Accordingly,  $\varrho$  and  $T_j(\varrho)$  decrease. Hence, the convergence rate of full GMRES decreases with  $E_b/N_0$ .  $\square$

Next, we discuss the convergence of restarted GMRES, which is slower than that of full GMRES [29]. This is due to the fact that once the algorithm is restarted, the current approximation subspace is discarded, and the residual generated later will not be orthogonal to the previously obtained subspace. Nevertheless, the convergence of restarted GMRES used in the MMSE estimator can still be guaranteed as stated in Theorem 2.

**Theorem 2.** *Restarted GMRES applied to MMSE estimation converges for any  $j_m \geq 1$ .*

*Proof.* The proof is given in the Appendix. □

### B. Complexity Analysis

In this subsection, we focus on the complexity of GMRES and FSPAI while neglecting other operations that take trivial computational time due to the inherent sparsity, such as  $\mathbf{L}\mathbf{L}^H$ ,  $\xi_n$ . Since the maximum degree of  $\mathbf{A}$  is  $\kappa$ , which has an order  $\mathcal{O}(P^2)$ , we prefer to use  $P$  as a reference to determine some other parameters, including  $j_m$ ,  $\zeta$ , and  $\epsilon_D$ .

According to [20], full GMRES has a complexity order  $\mathcal{O}((J + |\mathcal{D}|)JMN)$ , where  $|\mathcal{D}|$  is the number of nonzero elements in each column of  $\mathbf{A}$  and  $J$  denotes the number of iterations to reach the tolerance  $\epsilon_g$ . Typically,  $J$  is less than  $|\mathcal{D}|$ , and thus the complexity order is roughly  $\mathcal{O}(|\mathcal{D}|JMN)$ . For restarted GMRES, the complexity order reduces to  $\mathcal{O}((j_m + |\mathcal{D}|)j_mMN)$  per restart cycle, and hence  $\mathcal{O}(n_{cyc}(j_m + |\mathcal{D}|)j_mMN)$  in total, where  $n_{cyc}$  denotes the required number of restart cycles. Since generally  $j_m \ll |\mathcal{D}|$ , restarted GMRES has a complexity order  $\mathcal{O}(n_{cyc}|\mathcal{D}|j_mMN)$ .

In FSPAI, the computational complexity is dominated by computing the inverse  $\mathbf{A}(\tilde{\mathcal{C}}_k, \tilde{\mathcal{C}}_k)^{-1}$  of (35a). Since FSPAI aims to derive an approximation of the Cholesky factor of  $\mathbf{A}^{-1}$ , we focus on the sparsity level of  $\mathbf{L}$ . According to Algorithm 2, if a column of  $\mathbf{L}$  has a degree  $\varphi_L = D$ , the complexity order of this column is  $\mathcal{O}(D^4)$ . However, the practical degree  $D$  is quite problem-dependent, because the random matrix  $\mathbf{A}$  may lead to strikingly different sparsity level of  $\mathbf{L}$ . Nevertheless, with the aid of  $F_{\varphi_L}(D)$ , the average complexity is derived as  $\mathcal{O}(\sum_{D=1}^{\zeta} D^4 P(\varphi_L = D)MN/n_p) = \mathcal{O}(\mathbb{E}\{\varphi_L^4\}MN/n_p)$ , where  $n_p$  is the number of processors available for parallel computing and  $\zeta$  is the maximum node degrees of  $\mathbf{L}$  as given in Algorithm 2. Furthermore, the worst case of FSPAI, where each node has degree  $\zeta$ , has a complexity order  $\mathcal{O}(\zeta^4 MN/n_p)$ . Thus, even in the worst case, the complexity increases linearly with  $MN$ . As will be observed in the simulations,  $\zeta = P$  is sufficient, and  $\varphi_L$  typically concentrates around zero, especially at

high  $E_b/N_0$ . This indicates that  $\mathbf{L}$  is generally very sparse, and the average complexity is far less than that of the worst case.

## VII. SIMULATION RESULTS

In this section, the BER performance of OTFS with different detectors are simulated and discussed. Then, we analyze the convergence rate of full and restarted GMRES respectively. Thereafter, to evaluate the computational complexity of FSPA, we investigate the sparsity level of  $\mathbf{L}$ . We set  $M = 64$ ,  $N = 32$ , and the length of CP is  $L = 16$ . An  $R_c = 0.5$  convolutional code with generator (5,7) in octal is used. It is assumed that each path gain follows Rayleigh distribution with uniform power delay profile, i.e.,  $\mathbb{E}\{|h_p|^2\} = 1/P$ . The delay and Doppler indices are uniformly chosen such that  $0 \leq l \leq l_{\max}$  and  $-k_{\max} \leq k \leq k_{\max}$ , where  $l_{\max} = 10$  and  $k_{\max} = 6$ . Compared to the DI-S-MMSE turbo equalizer, the DI-S-MMSE equalizer is utilized for uncoded OTFS systems, where the MMSE estimator treats its own extrinsic information generated previously as the *a priori* information in the next outer iteration.

In Fig. 5 (a), the BER performance of OTFS system with our proposed DI-S-MMSE (turbo) receivers is presented. For comparison, the OTFS systems with LMMSE and sum-product algorithm (SPA) [30] detectors are also simulated, where the latter is a near-optimal symbol-wise MAP algorithm [10]. Due to the high complexity of SPA detector, we choose  $P = 4$ . At the first outer iteration, the DI-S-MMSE equalizer resorts to GMRES and achieves the same performance of the conventional LMMSE equalizer. After 5 outer iterations, the performance of the DI-S-MMSE equalizer has a roughly 4 dB gain compared to that of the LMMSE detector at around  $\text{BER} = 10^{-3}$ , and more importantly, it approaches the performance of the SPA detector. Furthermore, with the help of the decoder, the DI-S-MMSE turbo equalizer has a superior performance to the DI-S-MMSE equalizer, where the former has a roughly 2 dB gain compared to the SPA detector after 5 outer iterations at  $\text{BER} = 10^{-4}$ .

Fig. 5 (b) shows the BER performance of our proposed DI-S-MMSE (turbo) receivers with  $P = 8$ . To evaluate the performance loss, we present the BER performance of iterative MMSE (I-MMSE) and I-MMSE turbo receivers, where  $\mathbf{A}^{-1}$  is directly computed without resorting to GMRES and FSPA. Thus, the I-MMSE (turbo) receivers serve as lower bounds of our proposed receivers. It is found that there is no performance loss at the first outer iteration. On the other hand, at the subsequent outer iterations, the use of FSPA brings a marginal performance



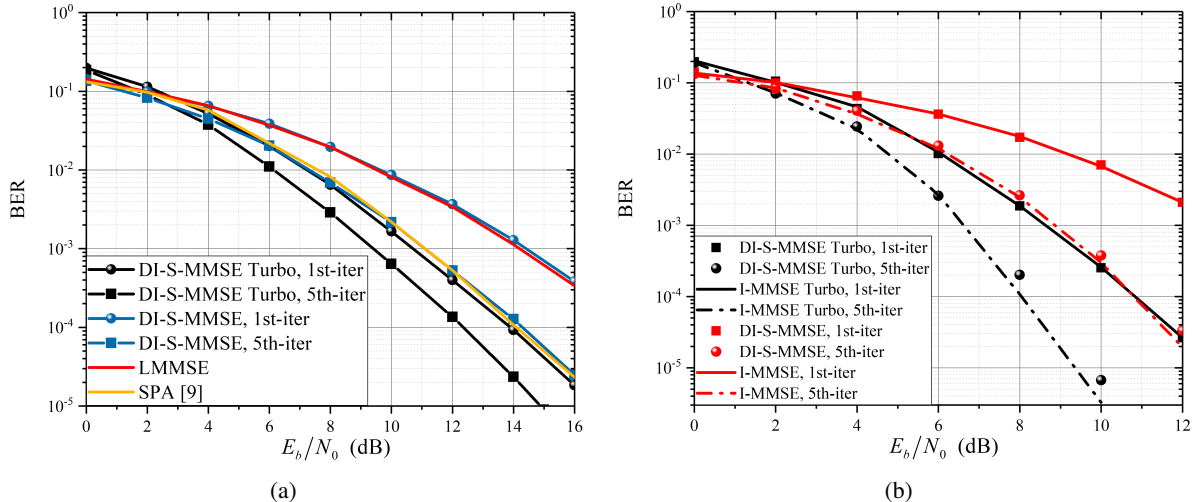


Fig. 5. The BER performance of our proposed DI-S-MMSE (turbo) equalizers, where  $\epsilon_g = \epsilon_f = \epsilon_A = 10^{-3}$ ,  $\epsilon_D = P/4$  and  $\zeta = P$ . (a) With  $P = 4$ , we present the BER performance of the LMMSE equalizer and SPA detector for comparison. (b) With  $P = 8$ , we simulate the BER performance of the I-MMSE (turbo) receivers as a lower bound, where  $\mathbf{A}^{-1}$  is directly computed.

degradation. There is around 0.2 dB performance loss after 5 outer iterations. Thus,  $\zeta = P$  is sufficient to avoid considerable performance loss.

Fig. 6 shows the convergence performance of full and restarted GMRES. In Fig. 6 (a), we investigate the average relative residual norms of full GMRES applied to two sparse linear systems and their upper bounds with the number of inner iterations, where GMRES1 and GMRES2 refer to linear systems  $\mathbf{A}\mathbf{f}_1 = \mathbf{y}$  and  $\mathbf{A}\mathbf{f}_2 = \mathbf{h}_n$  respectively. It is observed that full GMRES can converge steadily at any  $E_b/N_0$  in both sparse linear systems. In addition, the average relative residual norms of the upper bound have a gap compared to those of both linear systems, but they have the same slope. This clearly substantiates Theorem 1, where the upper bound provides a good approximation of the convergence rate. Furthermore, GMRES converges faster at a smaller  $E_b/N_0$ . For example, for GMRES1 and a given tolerance  $10^{-3}$ , around 15 inner iterations are required at  $E_b/N_0 = 6$  dB, while around 22 inner iterations are needed at  $E_b/N_0 = 10$  dB. This verifies the observation in Corollary 1.

Fig. 6 (b) shows the average relative residual norms of restarted GMRES applied to two sparse linear systems with the number of restart cycles at  $E_b/N_0 = 10$  dB, where the number of inner iterations of a restart cycle is set as  $j_m = P = 8$  and  $j_m = P/2 = 4$  respectively. We observe that the convergence of the current restart cycle tends to be slower than that of the previous one. For example, for GMRES1 with  $j_m = P/2$ , the average relative residual norms are reduced by around 90% (from 1 to around 0.1) at the first restart cycle, but around 70% (from 0.1 to 0.03) at

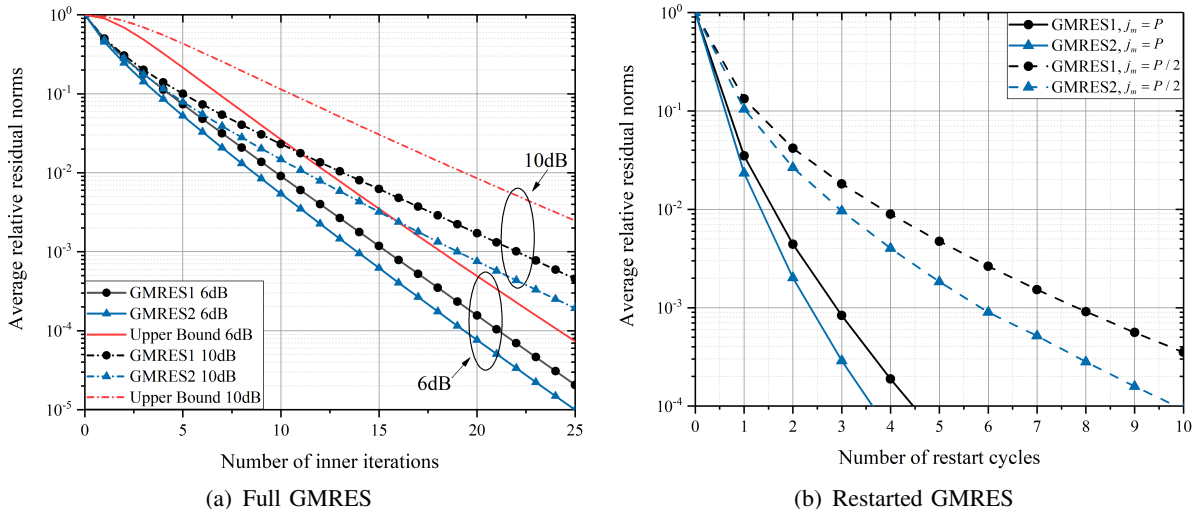


Fig. 6. Average relative residual norms of full and restarted GMRES applied to two linear systems, where  $P = 8$ . (a) Full GMRES cases and the corresponding upper bounds with the number of inner iterations at  $E_b/N_0 = 6$  dB and 10 dB. (b) Restarted GMRES cases with the number of restart cycles, where  $E_b/N_0 = 10$  dB.

the second restart cycle. Hence, the reduction of the residual norms of the current restart cycle is worse than that of the previous restart cycle, which is consistent with the convergence analysis. Furthermore, a smaller  $j_m$  results in a slower convergence, and a larger  $n_{cyc}$  is required to reach the drop tolerance  $\epsilon_g$ . For both linear systems with  $j_m = P$ ,  $n_{cyc} = 3$  is sufficient to reduce the residual norms to  $10^{-3}$ , while  $n_{cyc} = 8$  is sufficient for  $j_m = P/2$ . Nevertheless, the latter greatly reduces the complexity of each restart cycle compared to the former, since the maximum dimension of Krylov subspace is restricted. More importantly, regardless of the choice of  $j_m$ , restarted GMRES applied here can always converge, which demonstrates Theorem 2.

Then, Fig. 7 shows the sparsity level of  $\mathbf{L}$ , which largely determines the complexity of FSPA as analyzed in Section VI-B. From  $F_{\varphi_L}(D)$ , we can readily observe the distribution of  $\varphi_L$ , and derive the average complexity of FSPA. Fig. 7 (a) illustrates the CDF  $F_{\varphi_L}(D)$  of the second outer iteration at different  $E_b/N_0$  with  $P = 8$ . The drop tolerances of GMRES and FSPA are set to be  $\epsilon_g = \epsilon_f = 10^{-3}$ . The parameters of sparsification guidelines are chosen to be  $\epsilon_A = 10^{-3}$  and  $\epsilon_D = P/4$  respectively. The maximum degree of nodes  $\zeta = P = 8$  is sufficient to avoid noticeable performance loss. For the DI-S-MMSE turbo receiver at  $E_b/N_0 = 6$  dB,  $F_{\varphi_L}(P/2) \approx 0.75$  shows that around 75% nodes have degree not larger than  $P/2$ ; at  $E_b/N_0 = 10$  dB, we observe that  $F_{\varphi_L}(0) \approx 1$ , which indicates that most  $\varphi_L$  is zero and  $\mathbf{L}$  is nearly a diagonal matrix. This is due to the fact that with the increase of  $E_b/N_0$ , the extrinsic information generated by the decoder is more reliable. Thus, the new variances are closer to zero, and together with the

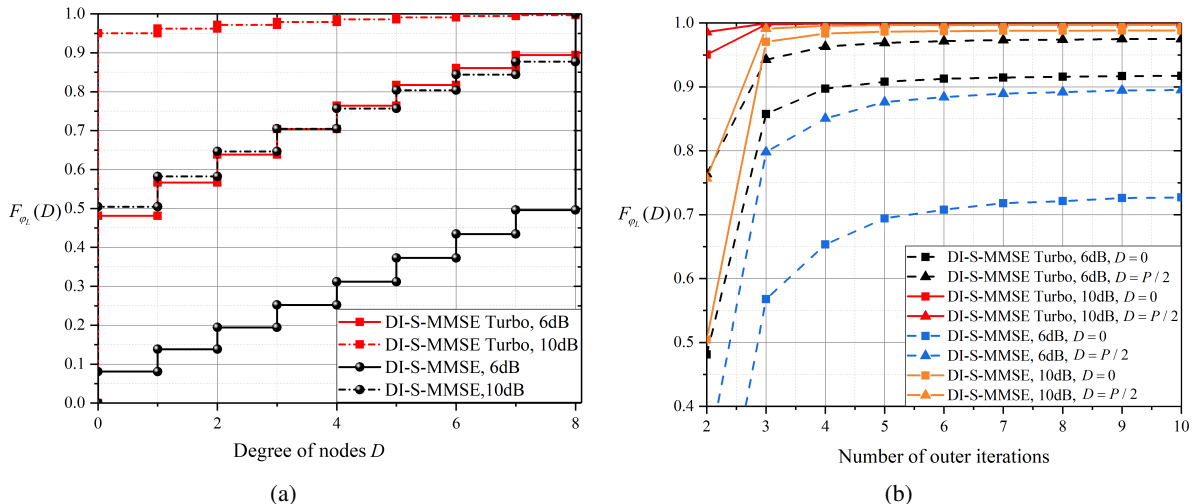


Fig. 7. The sparsity level of  $\mathbf{L}$ , measured by CDF  $F_{\varphi_L}(D)$ , where  $E_b/N_0 = 6$  dB and 10 dB with  $P = 8$ . (a) The sparsity level of  $\mathbf{L}$  at the second outer iteration. (b) The sparsity level of  $\mathbf{L}$  versus the number of outer iterations, and  $D$  is set to be 0 and  $P/2$  respectively.

sparsification guidelines applied to  $\mathbf{A}$ , a sparser approximation  $\mathbf{L}$  is made possible. Furthermore, at the same  $E_b/N_0$ ,  $\mathbf{L}$  of the DI-S-MMSE turbo receiver tends to be much sparser than that of the DI-S-MMSE receiver. This is demonstrated in the figure that  $F_{\varphi_L}(D)$  of the DI-S-MMSE turbo receiver is strictly larger than that of the DI-S-MMSE receiver, so that  $\mathbf{L}$  is sparser and requires less computation. Hence, the simulation results verify that FSPAI can indeed reduce the complexity substantially, and the reduction is more manifest with the help of the decoder.

Fig. 7 (b) shows the sparsity level of  $\mathbf{L}$  with the number of outer iterations at  $E_b/N_0 = 6$  dB and 10 dB, where  $P = 8$ , and  $D$  is chosen to be 0 and  $P/2$  respectively. Similarly,  $F_{\varphi_L}(D)$  of the DI-S-MMSE turbo receiver is strictly larger than that of the DI-S-MMSE receiver at the same  $E_b/N_0$ , which indicates that the proposed turbo receiver provides a smaller  $\varphi_L$  and thus a lower complexity. Besides,  $F_{\varphi_L}(D)$  increases with  $E_b/N_0$ . More importantly,  $F_{\varphi_L}(D)$  increases with the number of outer iterations, and the overall complexity of FSPAI is mainly dominated by the second outer iteration. This verifies that the *a priori* information is improved with the outer iteration, and the resultant new variances  $v_n$  are closer to zero, leading to a sparser  $\mathbf{L}$ . For example, at the third outer iteration and  $E_b/N_0 = 10$  dB, both receivers have  $F_{\varphi_L}(0) > 0.95$  and  $F_{\varphi_L}(P/2) \approx 1$ . Hence,  $\mathbf{L}$  is nearly diagonal, which has 95% nodes with degree zero and almost all the nodes with degree less than  $P/2$ . From Fig. 5 and Fig. 7, it is verified that the turbo structure not only improves the BER performance, but also greatly reduces the complexity. Therefore, the proposed DI-S-MMSE turbo equalizer can indeed achieve a great performance with a preferable complexity.

TABLE I  
COMPUTATIONAL COMPLEXITY OF DIFFERENT DETECTORS

Low complexity LMMSE equalizer [9]	$\mathcal{O}(\frac{MN}{2} \log_2 M + MN(2l_{max}^2 + 2P^2k_{max}))$
SPA detector [10]	$\mathcal{O}(n_{iter}MNP \mathcal{S} ^P)$
Our proposed equalizer	$\mathcal{O}(MN(n_{cyc} \mathcal{D} j_m + \frac{n_{iter}-1}{n_p} \mathbb{E}\{\varphi^4\}))$

The computational complexity of the aforementioned detectors is summarized in Table VII, where  $n_{iter}$  is the number of iterations of the SPA detector, and also the number of outer iterations of our proposed equalizer. In our proposed equalizer, we use restarted GMRES as an example and neglect the complexity of the decoder for a fair comparison. It is observed that our proposed equalizer has a complexity order linearly increasing with  $MN$ . Thus, compared to the LMMSE equalizer in [9], which has a log-linear order of complexity, our proposed equalizer lends itself to the OTFS systems that have a large frame size. On the other hand, since typically  $\zeta = P$  is sufficient, even in the worst case, the overall complexity order of our proposed equalizer increases with  $P^4$  as discussed in Section VI-B. However, as observed in Fig. 7, the average complexity is far less than the worst case. On the contrary, the complexity order of the SPA detector is exponential to  $P$ , which can be exceedingly high compared to our proposed equalizer in richly scattered environment with large  $P$ .

## VIII. CONCLUSION

This paper developed a DI-S-MMSE turbo equalizer. To exploit the inherent sparsity of the channel matrix, we resorted to graph theory to analyze the sparse matrices and proposed two sparsification guidelines. At the initial outer iteration, we applied GMRES to avoid directly computing the inverse of the covariance matrix with little performance loss. In addition, GMRES can be readily extended to other LMMSE systems if the covariance matrix is sparse. Then, we modified FSPA to derive an approximate inverse of the covariance matrix. Next, we proved the global convergence of full and restarted GMRES respectively, and demonstrated that the overall complexity order of our proposed equalizer increases linearly with the frame size. Simulation results demonstrated that our proposed equalizer can indeed deliver a great BER performance with a tremendously reduced complexity. In our future work, we will investigate how to mitigate the interference caused by fractional Doppler shifts with low complexity.

## APPENDIX

## PROOF OF THEOREM 2

After restarted GMRES performs  $j_m$  iterations, i.e., a restart cycle, the residual is given by

$$\|\mathbf{r}_{j_m}\| = \|\mathbf{r}_0 - \mathbf{A}\Delta\mathbf{f}'_{j_m}\| = \min_{\Delta\mathbf{f}'_{j_m} \in \mathcal{K}_{j_m}} \|\mathbf{r}_0 - \mathbf{A}\Delta\mathbf{f}'_{j_m}\|, \quad (44)$$

where  $\Delta\mathbf{f}'_{j_m}$  is the solution of the LS problem. Considering  $\Delta\mathbf{f}'_{j_m} \in \mathcal{K}_{j_m}$ ,  $\mathbf{A}\Delta\mathbf{f}'_{j_m}$  belongs to a subspace spanned by  $\{\mathbf{A}\mathbf{r}_0, \dots, \mathbf{A}^{j_m}\mathbf{r}_0\}$ . Then, from (44), the minimum residual is obtained when  $\mathbf{r}_{j_m}$  is perpendicular to this subspace and  $\mathbf{A}\Delta\mathbf{f}'_{j_m}$  is the projection of  $\mathbf{r}_0$  onto this subspace. Hence,  $\|\mathbf{r}_{j_m}\|^2 = \|\mathbf{r}_0\|^2 - \|\mathbf{A}\Delta\mathbf{f}'_{j_m}\|^2$ , and  $\mathbf{A}\Delta\mathbf{f}'_{j_m} = \mathbf{K}(\mathbf{K}^H\mathbf{K})^{-1}\mathbf{K}^H\mathbf{r}_0$  where  $\mathbf{K} = [\mathbf{A}\mathbf{r}_0, \dots, \mathbf{A}^{j_m}\mathbf{r}_0]$  [31]. Now, we have the relative residual

$$\|\mathbf{r}_{j_m}\|^2/\|\mathbf{r}_0\|^2 = 1 - \|\overline{\mathbf{K}}(\overline{\mathbf{K}}^H\overline{\mathbf{K}})^{-1}\overline{\mathbf{K}}^H\overline{\mathbf{r}}_0\|^2 = 1 - \overline{\mathbf{r}}_0^H\overline{\mathbf{K}}(\overline{\mathbf{K}}^H\overline{\mathbf{K}})^{-1}\overline{\mathbf{K}}^H\overline{\mathbf{r}}_0, \quad (45)$$

where  $\overline{\mathbf{r}}_0 = \mathbf{r}_0/\|\mathbf{r}_0\|$  and  $\overline{\mathbf{K}} = [\mathbf{A}\overline{\mathbf{r}}_0, \dots, \mathbf{A}^{j_m}\overline{\mathbf{r}}_0]$ . Then, the upper bound of (45) is given by

$$\frac{\|\mathbf{r}_{j_m}\|^2}{\|\mathbf{r}_0\|^2} \leq 1 - \overline{\mathbf{r}}_0^H\overline{\mathbf{K}}\overline{\mathbf{K}}^H\overline{\mathbf{r}}_0/\lambda_{\max}(\overline{\mathbf{K}}^H\overline{\mathbf{K}}) \stackrel{(a)}{\leq} 1 - \sum_{j=1}^{j_m} |\overline{\mathbf{r}}_0^H\mathbf{A}^j\overline{\mathbf{r}}_0|^2/\text{tr}(\overline{\mathbf{K}}^H\overline{\mathbf{K}}) = 1 - \varepsilon_{j_m}, \quad (46)$$

where (a) follows from the fact that  $\overline{\mathbf{K}}^H\overline{\mathbf{K}}$  is a Gram matrix and thus positive semidefinite. It is easy to know that  $\text{tr}(\overline{\mathbf{K}}^H\overline{\mathbf{K}}) > 0$ . On the other hand, since  $\mathbf{A}^j$  is HPD,  $\overline{\mathbf{r}}_0^H\mathbf{A}^j\overline{\mathbf{r}}_0 > 0$  for  $j \geq 1$  and any  $\overline{\mathbf{r}}_0$ . Hence, for any  $j_m \geq 1$ ,  $\varepsilon_{j_m}$  is always positive and thus the relative residual is less than one. This proves the global convergence of restarted GMRES.

## REFERENCES

- [1] R. Hadani, S. Rakib, M. Tsatsanis, A. Monk, A. J. Goldsmith, A. F. Molisch, and R. Calderbank, "Orthogonal time frequency space modulation," in *2017 IEEE Wireless Communications and Networking Conference (WCNC)*. IEEE, 2017, pp. 1–6.
- [2] R. Hadani and A. Monk, "OTFS: A new generation of modulation addressing the challenges of 5G," *arXiv preprint arXiv:1802.02623*, 2018.
- [3] P. Raviteja, K. T. Phan, Y. Hong, and E. Viterbo, "Interference cancellation and iterative detection for orthogonal time frequency space modulation," *IEEE Transactions on Wireless Communications*, vol. 17, no. 10, pp. 6501–6515, 2018.
- [4] G. Surabhi, R. M. Augustine, and A. Chockalingam, "On the diversity of uncoded OTFS modulation in doubly-dispersive channels," *IEEE Transactions on Wireless Communications*, vol. 18, no. 6, pp. 3049–3063, 2019.
- [5] S. Li, J. Yuan, W. Yuan, Z. Wei, B. Bai, and D. W. K. Ng, "Performance analysis of coded OTFS systems over high-mobility channels," *IEEE Transactions on Wireless Communications*, 2021.
- [6] S. K. Mohammed, "Derivation of OTFS Modulation From First Principles," *IEEE Transactions on Vehicular Technology*, vol. 70, no. 8, pp. 7619–7636, 2021.
- [7] P. Raviteja, K. T. Phan, and Y. Hong, "Embedded pilot-aided channel estimation for OTFS in delay–Doppler channels," *IEEE Transactions on Vehicular Technology*, vol. 68, no. 5, pp. 4906–4917, 2019.
- [8] K. Murali and A. Chockalingam, "On OTFS modulation for high-Doppler fading channels," in *2018 Information Theory and Applications Workshop (ITA)*. IEEE, 2018, pp. 1–10.

- [9] S. Tiwari, S. S. Das, and V. Rangamgari, “Low complexity LMMSE receiver for OTFS,” *IEEE Communications Letters*, vol. 23, no. 12, pp. 2205–2209, 2019.
- [10] S. Li, W. Yuan, Z. Wei, J. Yuan, B. Bai, D. W. K. Ng, and Y. Xie, “Hybrid MAP and PIC Detection for OTFS Modulation,” *IEEE Transactions on Vehicular Technology*, vol. 70, no. 7, pp. 7193–7198, 2021.
- [11] W. Yuan, Z. Wei, J. Yuan, and D. W. K. Ng, “A simple variational Bayes detector for orthogonal time frequency space (OTFS) modulation,” *IEEE Transactions on Vehicular Technology*, vol. 69, no. 7, pp. 7976–7980, 2020.
- [12] Z. Yuan, F. Liu, W. Yuan, Q. Guo, Z. Wang, and J. Yuan, “Iterative detection for orthogonal time frequency space modulation with unitary approximate message passing,” *IEEE Transactions on Wireless Communications*, 2021.
- [13] S. Li, W. Yuan, Z. Wei, and J. Yuan, “Cross domain iterative detection for orthogonal time frequency space modulation,” *arXiv preprint arXiv:2101.03822*, 2021.
- [14] P. Raviteja, Y. Hong, E. Viterbo, and E. Biglieri, “Practical pulse-shaping waveforms for reduced-cyclic-prefix OTFS,” *IEEE Transactions on Vehicular Technology*, vol. 68, no. 1, pp. 957–961, 2018.
- [15] H. V. Poor, *An introduction to signal detection and estimation*. Springer Science & Business Media, 2013.
- [16] M. Tuchler, A. C. Singer, and R. Koetter, “Minimum mean squared error equalization using a priori information,” *IEEE Transactions on Signal processing*, vol. 50, no. 3, pp. 673–683, 2002.
- [17] G. H. Golub and C. F. Van Loan, “Matrix computations. johns hopkins studies in the mathematical sciences,” 1996.
- [18] O. Østerby and Z. Zlatev, “Direct methods for sparse matrices,” *DAIMI Report Series*, no. 123, 1983.
- [19] M. Sedlacek, “Sparse approximate inverses for preconditioning, smoothing, and regularization,” Ph.D. dissertation, Technische Universität München, 2012.
- [20] Y. Saad and M. H. Schultz, “GMRES: A generalized minimal residual algorithm for solving nonsymmetric linear systems,” *SIAM Journal on scientific and statistical computing*, vol. 7, no. 3, pp. 856–869, 1986.
- [21] W. E. Arnoldi, “The principle of minimized iterations in the solution of the matrix eigenvalue problem,” *Quarterly of applied mathematics*, vol. 9, no. 1, pp. 17–29, 1951.
- [22] Y. Saad, *Iterative methods for sparse linear systems*. SIAM, 2003.
- [23] R. A. Horn and C. R. Johnson, *Matrix analysis*. Cambridge university press, 2012.
- [24] L. Y. Kolotilina and A. Y. Yeremin, “Factorized sparse approximate inverse preconditionings i. theory,” *SIAM Journal on Matrix Analysis and Applications*, vol. 14, no. 1, pp. 45–58, 1993.
- [25] I. E. Kaporin, “New convergence results and preconditioning strategies for the conjugate gradient method,” *Numerical linear algebra with applications*, vol. 1, no. 2, pp. 179–210, 1994.
- [26] T. Huckle, “Factorized sparse approximate inverses for preconditioning,” *The Journal of Supercomputing*, vol. 25, no. 2, pp. 109–117, 2003.
- [27] J. Liesen and P. Tichý, “Convergence analysis of Krylov subspace methods,” *GAMM-Mitteilungen*, vol. 27, no. 2, pp. 153–173, 2004.
- [28] Y. Saad, “Krylov subspace methods for solving large unsymmetric linear systems,” *Mathematics of computation*, vol. 37, no. 155, pp. 105–126, 1981.
- [29] A. H. Baker, E. R. Jessup, and T. Manteuffel, “A technique for accelerating the convergence of restarted GMRES,” *SIAM Journal on Matrix Analysis and Applications*, vol. 26, no. 4, pp. 962–984, 2005.
- [30] F. R. Kschischang, B. J. Frey, and H.-A. Loeliger, “Factor graphs and the sum-product algorithm,” *IEEE Transactions on information theory*, vol. 47, no. 2, pp. 498–519, 2001.
- [31] J. Zítko, “Generalization of convergence conditions for a restarted GMRES,” *Numerical Linear Algebra with Applications*, vol. 7, no. 3, pp. 117–131, 2000.